

Method for Solving Bang-Bang and Singular Optimal Control Problems using Adaptive Radau Collocation

Elisha R. Pager*

Anil V. Rao†

*University of Florida
Gainesville, FL 32611*

Abstract

A method is developed for solving bang-bang and singular optimal control problems using adaptive Legendre-Gauss-Radau (LGR) collocation. The method is divided into several parts. First, a structure detection method is developed that identifies switch times in the control and analyzes the corresponding switching function for segments where the solution is either bang-bang or singular. Second, after the structure has been detected, the domain is decomposed into multiple domains such that the multiple-domain formulation includes additional decision variables that represent the switch times in the optimal control. In domains classified as bang-bang, the control is set to either its upper or lower limit. In domains identified as singular, the objective function is augmented with a regularization term to avoid the singular arc. An iterative procedure is then developed for singular domains to obtain a control that lies in close proximity to the singular control. The method is demonstrated on five examples, four of which have either a bang-bang and/or singular optimal control while the fifth has a smooth and nonsingular optimal control. The results demonstrate that the method of this paper provides accurate solutions to problems whose solutions are either bang-bang or singular when compared against previously developed mesh refinement methods that are not tailored for solving nonsmooth and/or singular optimal control problems, and produces results that are equivalent to those obtained using previously developed mesh refinement methods for optimal control problems whose solutions are smooth.

1 Introduction

Optimal control problems arise in many engineering applications due to the need to optimize the performance of a controlled dynamical system. In general, optimal control problems do not have analytic solutions and must be solved numerically. A key challenge in solving an optimal control problem numerically arises due to the fact that most optimal control problems are subject to constraints on the system. These constraints often take the form of path constraints where limits are imposed on functions of either the control and/or the state. Constrained optimal control problems often have nonsmooth solutions, where the nonsmoothness arises in the forms of instantaneous switches in the control or switches between activity and inactivity in

*Ph.D. Candidate, Department of Mechanical and Aerospace Engineering, University of Florida, Gainesville, Florida 32611-6250. Email: epager@ufl.edu.

†Professor, Department of Mechanical and Aerospace Engineering, University of Florida, Gainesville, FL 32611-6250. E-mail: anilvrao@ufl.edu. Corresponding Author.

the state path constraints. Moreover, many constrained optimal control problems have solutions that lie on one or more singular arcs. The existence of a singular arc makes solving constrained optimal control problems even more challenging because Pontryagin’s minimum principle (that is, the first and second-order optimality conditions) fail to yield a complete solution along the singular arc. As a result, when applying a computational method to a problem whose solution lies on a singular arc, standard methods produce nonsensical results. This research is motivated by the importance of solving optimal control problems whose solutions are nonsmooth and singular.

Numerical methods for optimal control fall into two broad categories: indirect methods and direct methods. In an indirect method, the first-order variational optimality conditions are derived, and the optimal control problem is converted to a Hamiltonian boundary-value problem (HBVP). The HBVP is then solved numerically using a differential-algebraic equation solver. In a direct method, the state and control are approximated, and the optimal control problem is transcribed into a finite-dimensional nonlinear programming problem (NLP) [1]. The NLP is then solved numerically using well-developed software such as *SNOPT* [3] or *IPOPT* [2].

Over the past two decades, a particular class of direct methods, called direct collocation methods, has been used extensively for solving continuous optimal control problems. A direct collocation method is an implicit simulation method where the state and control are parameterized, and the constraints in the continuous optimal control problem are enforced at a specially chosen set of collocation points. In more recent years, a great deal of research has been carried out in the area of *Gaussian quadrature orthogonal collocation methods* [4, 5, 6, 7]. In a Gaussian quadrature collocation method, the state is approximated using a basis of Lagrange polynomials where the support points of the polynomials are chosen to be the points associated with a Gaussian quadrature. The most well developed Gaussian quadrature methods employ either Legendre-Gauss (LG) points [4, 8], Legendre-Gauss-Radau (LGR) points [5, 6, 7, 9, 10], or Legendre-Gauss-Lobatto (LGL) points [11]. More recently, a convergence theory has been developed to show that under certain assumptions of smoothness and coercivity, an *hp*-Gaussian quadrature method employing either LG or LGR collocation points will converge to a local minimizer of the optimal control problem at an exponential rate [12, 13, 14, 15, 16]. For these reasons, direct methods should be explored in the effort to develop novel computational methods for singular optimal control.

Computational issues arise when a solution to an optimal control problem is either nonsmooth or singular. The difficulty with such optimal control problem is twofold. First, the precise locations of any discontinuities and the structure of the control must be identified. Static mesh refinement methods that employ Gaussian quadrature have been developed recently as an initial attempt to locate (approximately) discontinuities in the solution [17, 18, 19]. Even more recently, the idea of using variable mesh refinement methods and structure detection methods has been developed [22, 23, 24, 25, 26]. Unlike static mesh refinement methods such as those found in Refs. [10, 20, 21], variable mesh refinement methods work by including parameters in the optimization that define the location of the discontinuities. The methods in Refs. [22, 23, 24] use the Lagrange multipliers to detect the switch point locations in the control structure and then place variable mesh points to represent the switch times in the NLP, while Refs. [25, 26] use the switching function and a sensitivity analysis to place moving finite elements at the switch point locations. Furthermore, Ref. [27] describes a mesh refinement method for solving bang-bang optimal control problems based on the switching function associated with the Hamiltonian. More recently, in Ref. [28] a switch point algorithm was developed for optimizing over the locations of switch points in a nonsmooth control solution, but a priori knowledge of the switch points existence is required. Finally, methods that utilize structure detection on a static mesh are described in Refs. [29, 30].

The second difficulty in solving optimal control problems with nonsmooth or singular solutions arises when the optimal control is singular. Several approaches have been developed for solving singular optimal control problems using both indirect and direct methods. A majority of these methods typically employ either a regularization approach or use of the optimality conditions with an indirect method to solve for the singular control (see Refs. [32, 33]). A regularization method transforms the singular control problem into a series of nonsingular problems by minimizing the sum of the original objective and a regularization term, where the regularization term is a quadratic function of the control. Regularization approaches have been implemented using dynamic programming, indirect methods, direct methods, and nested indirect/direct approaches as described in Refs. [31, 34, 35, 36]. More recent implementations of regularization based techniques include the uniform trigonumerization method (UTM) developed in [37] and the use of a continuation method of a regularized term in [38]. The UTM method is an indirect approach that uses regularization and trigonometric forms of the control to determine singular optimal control solutions. Aside from regularization

based approaches, research has also been conducted on the use of low-order representations of the control including straight line, monotonic, and nonmonotonic function approximations to reduce the oscillations and numerical challenges observed with singular arcs [39, 40].

Motivated by the prevalence of bang-bang and singular arcs in optimal control solutions and the need for a general method that can handle such solutions, this paper describes a new method for detecting and solving optimal control problems whose solutions are nonsmooth and singular. The method of this paper exploits the advantages of using a multiple-domain reformulation of LGR collocation with a regularization procedure to accurately detect and solve a singular optimal control problem. Identification of control switch times using jump function approximations [19] combined with identification of bang-bang and singular arcs is used to analyze the structure of a coarse control solution. The multiple-domain LGR collocation is used to partition the time horizon into domains with additional decision variables assigned at the identified switch time locations. Each type of domain is then constrained appropriately and hp -adaptive mesh refinement is utilized when necessary. More specifically, in a singular domain a regularization method, first introduced in [41, 42], is applied. The regularization method that is employed over a singular arc is developed as a variation of the $\epsilon\text{-}\alpha(\cdot)$ method presented in [34], but this paper extends the use of a regularization method to collocation methods. This research described in this paper also uses the Hamiltonian in the structure detection process, but differs from the method in [27] because this work can also detect and approximate singular arcs. In [27], singular arcs are not considered. Additionally, this work uses a different discontinuity detection method to first locate the switch times. Furthermore, the work presented in this paper differs from the work described in Ref. [34] in two ways. First, in this previous work the singular control is regularized and solved by iterative dynamic programming. Different from this prior research, in this work the regularization method is implemented by a direct method referred to as multiple-domain LGR collocation. Second, in this current research the regularization method developed is only applied over the time domain containing a singular arc as opposed to the entire time horizon.

The contributions of this work are as follows. First, using jump function approximations provides an accurate way to determine the number of discontinuities along with accurate estimates of the locations of these discontinuities. Second, using the switching function and the Hamiltonian enables determining those intervals where the control is either bang-bang or singular. Third, the method automatically partitions the

solution into domains based on the results of the structure detection method. Fourth, the method does not require any a priori knowledge of the structure in the optimal control or whether the optimal control is bang-bang or singular. Fifth, in this paper the use of regularization methods is extended to direct collocation methods. In particular, the multiple-domain partition of the solution obtained from the structure detection method enables regularizing only over those domains where the control is singular. Consequently, within a singular domain the regularization leads to a control that lies in close proximity to the singular control while simultaneously eliminating the need to derive the singular control conditions (where deriving such conditions may prove to be intractable depending upon the problem). The performance of the method developed in this paper is demonstrated on five examples. The optimal control for each of the first four of these examples is either bang-bang and/or singular, while the optimal control for the fifth example is smooth. The numerical results obtained of the first four examples demonstrate that the method of this paper produces significantly more accurate results when compared against mesh refinement methods that are not developed for solving optimal control problems whose solutions are nonsmooth or singular. Finally, the numerical results of the fifth example demonstrate the method of this paper correctly identifies when a solution is smooth and applies only static mesh refinement in order to obtain a solution. As a result, results comparable to those obtained using previously developed mesh refinement methods are obtained.

The remainder of the paper is organized as follows. Section 2 introduces the Bolza optimal control problem and the necessary conditions for optimality. Section 3 describes the multiple-domain Legendre-Gauss-Radau collocation used to transcribe the multiple-domain Bolza optimal control problem. Section 4 provides a brief overview of optimal control problems whose solutions are nonsmooth. Section 5 details the method for solving bang-bang and singular optimal control problems. Section 6 provides numerical solutions obtained by demonstrating the method on five examples. Section 7 provides a brief discussion of the results described in Section 6. Finally, Section 8 provides conclusions on this research.

2 Bolza Optimal Control Problem

Without loss of generality, consider the following single-phase optimal control problem in Bolza form defined on the time horizon $t \in [t_0, t_f]$. Determine the state $\mathbf{x}(t) \in \mathbb{R}^{n_x}$, the control $\mathbf{u}(t) \in \mathbb{R}^{n_u}$, and the terminal

time $t_f \in \mathbb{R}$ that minimize the objective functional

$$\mathcal{J} = \mathcal{M}(\mathbf{x}(t_0), t_0, \mathbf{x}(t_f), t_f) + \int_{t_0}^{t_f} \mathcal{L}(\mathbf{x}(t), \mathbf{u}(t), t) dt, \quad (1)$$

subject to the dynamic constraints

$$\frac{d\mathbf{x}(t)}{dt} \equiv \dot{\mathbf{x}}(t) = \mathbf{a}(\mathbf{x}(t), \mathbf{u}(t), t), \quad (2)$$

the path constraints

$$\mathbf{c}_{\min} \leq \mathbf{c}(\mathbf{x}(t), \mathbf{u}(t), t) \leq \mathbf{c}_{\max}, \quad (3)$$

the control constraints

$$\mathbf{u}_{\min} \leq \mathbf{u}(t) \leq \mathbf{u}_{\max}, \quad (4)$$

and the boundary conditions

$$\mathbf{b}_{\min} \leq \mathbf{b}(\mathbf{x}(t_0), t_0, \mathbf{x}(t_f), t_f) \leq \mathbf{b}_{\max}, \quad (5)$$

where the functions \mathcal{M} , \mathcal{L} , \mathbf{a} , \mathbf{b} , and \mathbf{c} are defined by the mappings

$$\mathcal{M} : \mathbb{R}^{n_x} \times \mathbb{R} \times \mathbb{R}^{n_x} \times \mathbb{R} \rightarrow \mathbb{R},$$

$$\mathcal{L} : \mathbb{R}^{n_x} \times \mathbb{R}^{n_u} \times \mathbb{R} \rightarrow \mathbb{R},$$

$$\mathbf{a} : \mathbb{R}^{n_x} \times \mathbb{R}^{n_u} \times \mathbb{R} \rightarrow \mathbb{R}^{n_x},$$

$$\mathbf{c} : \mathbb{R}^{n_x} \times \mathbb{R}^{n_u} \times \mathbb{R} \rightarrow \mathbb{R}^{n_c}.$$

$$\mathbf{b} : \mathbb{R}^{n_x} \times \mathbb{R} \times \mathbb{R}^{n_x} \times \mathbb{R} \rightarrow \mathbb{R}^{n_b}.$$

The Bolza optimal control problem given in Eqs. (1)–(5) gives rise to the following first-order calculus of variations [43, 44, 45] conditions:

$$\dot{\mathbf{x}}^\top(t) = \frac{\partial \mathcal{H}}{\partial \boldsymbol{\lambda}} = \mathcal{H}_{\boldsymbol{\lambda}}, \quad (6)$$

$$\dot{\boldsymbol{\lambda}}^\top(t) = -\frac{\partial \mathcal{H}}{\partial \mathbf{x}} = -\mathcal{H}_{\mathbf{x}}, \quad (7)$$

$$\mathbf{0} = \frac{\partial \mathcal{H}}{\partial \mathbf{u}} = \mathcal{H}_{\mathbf{u}}, \quad (8)$$

where $\boldsymbol{\lambda}(t) \in \mathbb{R}^{n_x}$ is the costate, $\boldsymbol{\mu}(t) \in \mathbb{R}^{n_c}$ is the path constraint multiplier,

$$\mathcal{H}(\mathbf{x}(t), \mathbf{u}(t), \boldsymbol{\lambda}(t), \boldsymbol{\mu}(t), t) = \mathcal{L}(\mathbf{x}(t), \mathbf{u}(t), t) + \boldsymbol{\lambda}^\top(t) \mathbf{a}(\mathbf{x}(t), \mathbf{u}(t), t) - \boldsymbol{\mu}^\top(t) \mathbf{c}(\mathbf{x}(t), \mathbf{u}(t), t), \quad (9)$$

is the augmented Hamiltonian, and \mathcal{U} is the admissible control set. Finally, the transversality conditions are given by

$$\boldsymbol{\lambda}(t_0) = -\frac{\partial \mathcal{M}}{\partial \mathbf{x}(t_0)} + \boldsymbol{\nu}^\top \frac{\partial \mathbf{b}}{\partial \mathbf{x}(t_0)} \quad , \quad \boldsymbol{\lambda}(t_f) = \frac{\partial \mathcal{M}}{\partial \mathbf{x}(t_f)} - \boldsymbol{\nu}^\top \frac{\partial \mathbf{b}}{\partial \mathbf{x}(t_f)} \quad (10)$$

$$\mathcal{H}(t_0) = \frac{\partial \mathcal{M}}{\partial t_0} - \boldsymbol{\nu}^\top \frac{\partial \mathbf{b}}{\partial t_0} \quad , \quad \mathcal{H}(t_f) = -\frac{\partial \mathcal{M}}{\partial t_f} + \boldsymbol{\nu}^\top \frac{\partial \mathbf{b}}{\partial t_f} \quad (11)$$

$$\mu_j(t) = 0, \text{ when } c_j(\mathbf{x}, \mathbf{u}, t) < 0, \quad j = 1, \dots, p \quad (12)$$

$$\mu_j(t) \leq 0, \text{ when } c_j(\mathbf{x}, \mathbf{u}, t) = 0, \quad j = 1, \dots, p$$

where $\boldsymbol{\nu}$ is the Lagrange multiplier associated with the boundary conditions. Equations (6) and (7) form what is classically known as a *Hamiltonian system* [43, 44]. The conditions in Eqs. (10) and (11) are called *transversality conditions* [43, 44, 45] on the boundary values of the costate, while the conditions given in Eq. (12) are the *complementary slackness conditions* [47, 48] on the path constraints. For some problems, the control cannot be uniquely determined, either implicitly or explicitly, from the optimality conditions given in Eqs. (6)–(12). In such cases, the weak form of Pontryagin’s minimum principle can be used which solves for the permissible control that minimizes the Hamiltonian in Eq. (9). If \mathcal{U} is the set of permissible controls, then Pontryagin’s minimum principle states that the optimal control, $\mathbf{u}(t)$, satisfies the condition

$$\mathcal{H}(\mathbf{x}^*(t), \mathbf{u}^*(t), \boldsymbol{\lambda}^*(t), \boldsymbol{\mu}^*(t), t) \leq \mathcal{H}(\mathbf{x}^*(t), \mathbf{u}, \boldsymbol{\lambda}^*(t), \boldsymbol{\mu}^*(t), t), \quad \mathbf{u} \in \mathcal{U}. \quad (13)$$

The Hamiltonian system, together with the original boundary conditions, the costate transversality conditions, and complementary slackness conditions, forms a *Hamiltonian boundary-value problem* (HBVP) [43, 44, 45]. Any solution $(\mathbf{x}^*(t), \mathbf{u}^*(t), \boldsymbol{\lambda}^*(t), \boldsymbol{\mu}^*(t), \boldsymbol{\nu}^*)$ to the HBVP is called an *extremal* solution.

3 Multiple-Domain Legendre-Gauss-Radau Collocation

In this paper, the previously developed *hp*-adaptive Legendre-Gauss-Radau (LGR) collocation method [5, 6, 7, 9, 10] is used to approximate the optimal control problem (where the term LGR collocation will be used from this point onwards to mean *hp*-adaptive Legendre-Gauss-Radau collocation). LGR collocation is used because it has been shown to converge at an exponential rate to a local solution of the optimal control problem for problems where the solution is smooth [13, 14, 15, 16]. The focus of this paper, however, is on solving optimal control problems whose solutions are nonsmooth and/or singular. As a result, modifications

to the standard LGR formulation are made. Specifically, a multiple-domain reformulation of LGR collocation is developed as described in the remainder of this section.

The multiple-domain formulation of LGR collocation divides the domain $t \in [t_0, t_f]$ into distinct partitions such that the endpoints of each partition are decision variables. The division into domains is obtained using a structure decomposition method as described in Section 5.1. The continuous-time Bolza optimal control problem described in Eqs. (1)–(5) is discretized using collocation at the Legendre-Gauss-Radau (LGR) points [5, 6, 7, 9]. The time horizon $t \in [t_0, t_f]$ may be divided into D time domains, $\mathcal{P}_d = [t_s^{[d-1]}, t_s^{[d]}] \subseteq [t_0, t_f]$, $d \in \{1, \dots, D\}$, such that

$$\bigcup_{d=1}^D \mathcal{P}_d = [t_0, t_f], \quad \bigcap_{d=1}^D \mathcal{P}_d = \{t_s^{[1]}, \dots, t_s^{[D-1]}\}, \quad (14)$$

where $t_s^{[d]}$, $d \in \{1, \dots, D-1\}$ are the domain interface variables of the problem, $t_s^{[0]} = t_0$, and $t_s^{[D]} = t_f$. Thus, in the case where $D = 1$ the phase consists of only a single domain $\mathcal{P}_1 = [t_0, t_f]$ and $\{t_s^{[1]}, \dots, t_s^{[D-1]}\} = \emptyset$.

$$\begin{aligned} t &= \frac{t_s^{[d]} - t_s^{[d-1]}}{2} \tau + \frac{t_s^{[d]} + t_s^{[d-1]}}{2}, \\ \tau &= 2 \frac{t - t_s^{[d-1]}}{t_s^{[d]} - t_s^{[d-1]}} - 1. \end{aligned} \quad (15)$$

The interval $\tau \in [-1, +1]$ for each domain \mathcal{P}_d is then divided into K mesh intervals, $\mathcal{I}_k = [T_{k-1}, T_k] \subseteq [-1, +1]$, $k \in \{1, \dots, K\}$ such that

$$\bigcup_{k=1}^K \mathcal{I}_k = [-1, +1], \quad \bigcap_{k=1}^K \mathcal{I}_k = \{T_1, \dots, T_{K-1}\}, \quad (16)$$

and $-1 = T_0 < T_1 < \dots < T_{K-1} < T_K = +1$. For each mesh interval, the LGR points used for collocation are defined in the domain of $[T_{k-1}, T_k]$ for $k \in \{1, \dots, K\}$. The state of the continuous optimal control problem is then approximated in mesh interval \mathcal{I}_k , $k \in \{1, \dots, K\}$, as

$$\mathbf{x}^{(k)}(\tau) \approx \mathbf{X}^{(k)}(\tau) = \sum_{j=1}^{N_k+1} \mathbf{X}_j^{(k)} \ell_j^{(k)}(\tau), \quad \ell_j^{(k)}(\tau) = \prod_{\substack{l=1 \\ l \neq j}}^{N_k+1} \frac{\tau - \tau_l^{(k)}}{\tau_j^{(k)} - \tau_l^{(k)}}, \quad (17)$$

where $\ell_j^{(k)}(\tau)$ for $j \in \{1, \dots, N_k + 1\}$ is a basis of Lagrange polynomials on \mathcal{I}_k , $(\tau_1^{(k)}, \dots, \tau_{N_k}^{(k)})$ are the set of N_k Legendre-Gauss-Radau (LGR) collocation points in the interval $[T_{k-1}, T_k]$, $\tau_{N_k+1}^{(k)} = T_k$ is a non-collocated support point, and $\mathbf{X}_j^{(k)} \equiv \mathbf{X}^{(k)}(\tau_j^{(k)})$. Differentiating $\mathbf{X}^{(k)}(\tau)$ in Eq. (17) with respect to τ gives

$$\frac{d\mathbf{X}^{(k)}(\tau)}{d\tau} = \sum_{j=1}^{N_k+1} \mathbf{X}_j^{(k)} \frac{d\ell_j^{(k)}(\tau)}{d\tau}. \quad (18)$$

The dynamics are then approximated at the N_k LGR points in mesh interval $k \in \{1, \dots, K\}$ as

$$\sum_{j=1}^{N_k+1} D_{lj}^{(k)} \mathbf{X}_j^{(k)} - \frac{t_f - t_0}{2} \mathbf{a} \left(\mathbf{X}_l^{(k)}, \mathbf{U}_l^{(k)}, t(\tau_l^{(k)}, t_0, t_f) \right) = \mathbf{0}, \quad l \in \{1, \dots, N_k\}, \quad (19)$$

where

$$D_{lj}^{(k)} = \frac{d\ell_j^{(k)}(\tau_l^{(k)})}{d\tau}, \quad l \in \{1, \dots, N_k\}, \quad j \in \{1, \dots, N_k + 1\},$$

are the elements of the $N_k \times (N_k + 1)$ *Legendre-Gauss-Radau differentiation matrix* in mesh interval \mathcal{I}_k , $k \in \{1, \dots, K\}$, and $\mathbf{U}_l^{(k)}$ is the approximation of the control at the l^{th} collocation point in mesh interval \mathcal{I}_k . The time variables t_0 and t_f in Eq. (19) represent the initial and final domain interface variables, $t_s^{[d-1]}$ and $t_s^{[d]}$, on the domain \mathcal{P}_d . It is noted that continuity in the state and time between mesh intervals \mathcal{I}_{k-1} and \mathcal{I}_k , $k \in \{1, \dots, K\}$, is enforced by using the same variables to represent $\mathbf{X}_{N_{k-1}+1}^{(k-1)}$ and $\mathbf{X}_1^{(k)}$, while continuity in the state between the domains \mathcal{P}_{d-1} and \mathcal{P}_d , $d \in \{2, \dots, D\}$, is achieved by using the same variables to represent $\mathbf{X}_{N^{[d-1]}+1}^{[d-1]}$ and $\mathbf{X}_1^{[d]}$ where the superscript $[d]$ is used to denote the d^{th} time domain, $\mathbf{X}_j^{[d]}$ denotes the value of the state approximation at the j^{th} discretization point in the time domain \mathcal{P}_d , and $N^{[d]}$ is the total number of collocation points used in time domain \mathcal{P}_d computed by

$$N^{[d]} = \sum_{k=1}^{K^{[d]}} N_k^{[d]}. \quad (20)$$

The Legendre-Gauss-Radau approximation of the multiple-domain optimal control problem results in the following nonlinear programming problem (NLP). Minimize the objective function

$$\mathcal{J} = \mathcal{M}(\mathbf{X}_1^{[1]}, t_0, \mathbf{X}_{N^{[D]}+1}^{[D]}, t_f) + \sum_{d=1}^D \frac{t_s^{[d]} - t_s^{[d-1]}}{2} \left[\mathbf{w}^{[d]} \right]^\top \mathbf{L}^{[d]}, \quad (21)$$

subject to the collocated dynamic constraints

$$\Delta^{[d]} = \mathbf{D}^{[d]} \mathbf{X}^{[d]} - \frac{t_s^{[d]} - t_s^{[d-1]}}{2} \mathbf{A}^{[d]} = \mathbf{0}, \quad d \in \{1, \dots, D\}, \quad (22)$$

the path constraints

$$\mathbf{c}_{\min} \leq \mathbf{C}_j^{[d]} \leq \mathbf{c}_{\max}, \quad j \in \{1, \dots, N^{[d]}\}, \quad d \in \{1, \dots, D\}, \quad (23)$$

the control constraints

$$\mathbf{u}_{\min} \leq \mathbf{U}_j^{[d]} \leq \mathbf{u}_{\max}, \quad j \in \{1, \dots, N^{[d]}\}, \quad d \in \{1, \dots, D\}, \quad (24)$$

the boundary conditions

$$\mathbf{b}_{\min} \leq \mathbf{b}(\mathbf{X}_1^{[1]}, t_0, \mathbf{X}_{N^{[D]}+1}^{[D]}, t_f) \leq \mathbf{b}_{\max} . \quad (25)$$

and the continuity constraints

$$\mathbf{X}_{N^{[d-1]}+1}^{[d-1]} = \mathbf{X}_1^{[d]}, \quad d \in \{2, \dots, D\} , \quad (26)$$

noting that Eq. (26) is implicitly satisfied by employing the same variable in the NLP for $\mathbf{X}_{N^{[d-1]}+1}^{[d-1]}$ and $\mathbf{X}_1^{[d]}$. The matrices in Eqs. (21)–(23) are defined as follows

$$\mathbf{A}^{[d]} = \begin{bmatrix} \mathbf{a}(\mathbf{X}_1^{[d]}, \mathbf{U}_1^{[d]}, t_1^{[d]}) \\ \vdots \\ \mathbf{a}(\mathbf{X}_{N^{[d]}}^{[d]}, \mathbf{U}_{N^{[d]}}^{[d]}, t_{N^{[d]}}^{[d]}) \end{bmatrix} \in \mathbb{R}^{N^{[d]} \times n_x} , \quad (27)$$

$$\mathbf{C}^{[d]} = \begin{bmatrix} \mathbf{c}(\mathbf{X}_1^{[d]}, \mathbf{U}_1^{[d]}, t_1^{[d]}) \\ \vdots \\ \mathbf{c}(\mathbf{X}_{N^{[d]}}^{[d]}, \mathbf{U}_{N^{[d]}}^{[d]}, t_{N^{[d]}}^{[d]}) \end{bmatrix} \in \mathbb{R}^{N^{[d]} \times n_c} , \quad (28)$$

$$\mathbf{L}^{[d]} = \begin{bmatrix} \mathcal{L}(\mathbf{X}_1^{[d]}, \mathbf{U}_1^{[d]}, t_1^{[d]}) \\ \vdots \\ \mathcal{L}(\mathbf{X}_{N^{[d]}}^{[d]}, \mathbf{U}_{N^{[d]}}^{[d]}, t_{N^{[d]}}^{[d]}) \end{bmatrix} \in \mathbb{R}^{N^{[d]} \times 1} , \quad (29)$$

$\mathbf{D}^{[d]} \in \mathbb{R}^{N^{[d]} \times [N^{[d]}+1]}$ is the LGR differentiation matrix in time domain \mathcal{P}_d , $d \in \{1, \dots, D\}$, and $\mathbf{w}^{[d]} \in \mathbb{R}^{N^{[d]} \times 1}$ are the LGR weights at each node in time domain \mathcal{P}_d , $d \in \{1, \dots, D\}$. It is noted that $\mathbf{a} \in \mathbb{R}^1 \times n_x$, $\mathbf{c} \in \mathbb{R}^1 \times n_c$, and $\mathcal{L} \in \mathbb{R}^1 \times 1$ correspond, respectively, to the vector fields that define the right-hand side of the dynamics, the path constraints, and the integrand of the optimal control problem, where n_c is the number of path constraints in the problem. Additionally, the state matrix, $\mathbf{X}^{[d]} \in \mathbb{R}^{[N^{[d]}+1] \times n_x}$, and the control matrix, $\mathbf{U}^{[d]} \in \mathbb{R}^{N^{[d]} \times n_u}$, in time domain \mathcal{P}_d , $d \in \{1, \dots, D\}$, are formed as

$$\mathbf{X}^{[d]} = \begin{bmatrix} \mathbf{X}_1^{[d]} \\ \vdots \\ \mathbf{X}_{N^{[d]}+1}^{[d]} \end{bmatrix} \quad \text{and} \quad \mathbf{U}^{[d]} = \begin{bmatrix} \mathbf{U}_1^{[d]} \\ \vdots \\ \mathbf{U}_{N^{[d]}}^{[d]} \end{bmatrix} , \quad (30)$$

respectively, where n_u is the number of control components and n_x is the number of state components in the problem.

3.1 Costate Estimation

Estimates of the costate may be obtained at each of the discretization points in the time domain $\mathcal{P}_d, d \in \{1, \dots, D\}$ using the transformation [5, 6, 7],

$$\begin{aligned}\boldsymbol{\lambda}^{[d]} &= (\mathbf{W}^{[d]})^{-1} \boldsymbol{\Lambda}^{[d]}, \\ \boldsymbol{\lambda}_{N^{[d]}+1}^{[d]} &= (\mathbf{D}_{N^{[d]}+1}^{[d]})^\top \boldsymbol{\Lambda}^{[d]},\end{aligned}\tag{31}$$

where $\boldsymbol{\lambda}^{[d]} \in \mathbb{R}^{N^{[d]} \times n_x}$ is a matrix of the costate estimates at the collocation points in time domain \mathcal{P}_d , $\mathbf{W}^{[d]} = \text{diag}(\mathbf{w}^{[d]})$ is a diagonal matrix of the LGR weights at the collocation points in time domain \mathcal{P}_d , $\boldsymbol{\Lambda}^{[d]} \in \mathbb{R}^{N^{[d]} \times n_x}$ is a matrix of the NLP multipliers obtained from the NLP solver corresponding to the defect constraints at the collocation points in time domain \mathcal{P}_d , $\boldsymbol{\lambda}_{N^{[d]}+1}^{[d]} \in \mathbb{R}^1 \times n_x$ is a row vector of the costate estimates at the non-located end point in time domain \mathcal{P}_d , and $\mathbf{D}_{N^{[d]}+1}^{[d]} \in \mathbb{R}^{N^{[d]} \times 1}$ is the last column of the LGR differentiation matrix in time domain \mathcal{P}_d .

The aforementioned multiple-domain LGR formulation is summarized as follows. First, a single *phase* problem on $t \in [t_0, t_f]$ is divided into D domains, $\mathcal{P}_d = [t_s^{[d-1]}, t_s^{[d]}]$, $d \in \{1, \dots, D\}$. Each of the D domains are then mapped to the interval $\tau^{[d]} \in [-1, +1]$, $d \in \{1, \dots, D\}$. The interval $\tau^{[d]} \in [-1, +1]$, $d \in \{1, \dots, D\}$ for each domain is then divided into K mesh intervals, $\mathcal{I}_k = [T_{k-1}, T_k] \subseteq [-1, +1]$, $k \in \{1, \dots, K\}$. Finally, the intersection of each domain is determined by the *domain interface variables*, $t_s^{[d]}$, $d \in \{1, \dots, D-1\}$.

4 Nonsmooth and Singular Optimal Control

The term nonsmooth is used to denote the optimal control as displaying both nonsmooth and singular behavior. By definition a singular arc will occur in a solution when the application of Pontryagin's minimum principle fails to yield a complete solution of the optimal control [45]. This phenomena can occur in many situations but is most common when the dynamics are linear in the control and the control is bounded, or the Hamiltonian is not an explicit function of time. It should be noted that singular arcs can also occur in other situations, but in order to provide structure to the method developed in this paper, only problems that fall into the aforementioned categories will be considered.

For simplicity, it is assumed that the control is scalar, $u(t) \in \mathbb{R}$, but the following discussion can be extended to multiple control components as shown in the examples provided in Section 6. Suppose the

optimal control problem described in Eqs. (1)–(5) is nonsmooth and singular as defined by the assumptions mentioned previously. The dynamics can now be rewritten in the affine form as

$$\dot{\mathbf{x}}(t) = \mathbf{a}(\mathbf{x}(t), u(t)) = \mathbf{g}(\mathbf{x}(t)) + \mathbf{h}(\mathbf{x}(t))u(t), \quad (32)$$

where $\mathbf{g}(\mathbf{x}(t))$ and $\mathbf{h}(\mathbf{x}(t))$ are not functions of the control. The Hamiltonian from Eq. (9) is redefined as

$$\mathcal{H}(\mathbf{x}(t), \boldsymbol{\lambda}(t), \boldsymbol{\mu}(t), u(t), t) = \mathbf{f}(\mathbf{x}(t), \boldsymbol{\lambda}(t)) + \phi^\top(\mathbf{x}(t), \boldsymbol{\lambda}(t))u(t) + \boldsymbol{\mu}^\top(t)\mathbf{c}(\mathbf{x}(t), t), \quad (33)$$

where $\mathbf{f}(\mathbf{x}(t), \boldsymbol{\lambda}(t))$ and $\phi(\mathbf{x}(t), \boldsymbol{\lambda}(t))$ are the components of the Hamiltonian that are not a function of the control, and mixed state and control path constraints are not considered. The strong form of Pontryagin's Minimum Principle (PMP), Eq. (13), is applied as follows

$$\frac{\partial \mathcal{H}}{\partial u} = \mathcal{H}_u = \phi(\mathbf{x}(t), \boldsymbol{\lambda}(t)) = 0. \quad (34)$$

Note that the control does not appear in Eq. (34) because the Hamiltonian is linear in the control. A singular arc is characterized as $\mathcal{H}_u = 0$ and \mathcal{H}_{uu} is singular everywhere on the arc. When this occurs, the reduced Hessian matrix associated with the corresponding NLP that arises from the direct transcription method of Section 3 is ill-conditioned such that the projected Hessian matrix is not positive definite. This leads to poor conditioning in the control profiles which often presents itself in the form of oscillations, or chattering behavior, in the control solution.

The sign and value of $\phi(\mathbf{x}(t), \boldsymbol{\lambda}(t))$ (where ϕ is called the switching function) determines if the control is called a *bang-bang* control or a *singular* control. The weak form of PMP [45] is used in the case of nonsmooth control and the minimization of the Hamiltonian leads to the following piecewise-continuous control, $u(t)$, that is dependent on the switching function as follows

$$u^*(t) = \arg \min_{u(t) \in \mathcal{U}} \mathcal{H} = \begin{cases} u_{\min} & , \quad \phi(\mathbf{x}(t), \boldsymbol{\lambda}(t)) > 0, \\ u_{\text{singular}} & , \quad \phi(\mathbf{x}(t), \boldsymbol{\lambda}(t)) = 0, \\ u_{\max} & , \quad \phi(\mathbf{x}(t), \boldsymbol{\lambda}(t)) < 0, \end{cases} \quad (35)$$

where the sign of the switching function, $\phi(\mathbf{x}(t), \boldsymbol{\lambda}(t))$, is determined by the state and the costate, and $\mathcal{U} \in [u_{\min}, u_{\max}]$ is the admissible control set. As the switching function $\phi(\mathbf{x}(t), \boldsymbol{\lambda}(t))$ changes sign, the control coincides with the sign changes by switching between its maximum and minimum values. Any time interval over which $\phi(\mathbf{x}(t), \boldsymbol{\lambda}(t))$ is zero is referred to as a singular arc and any control in the admissible

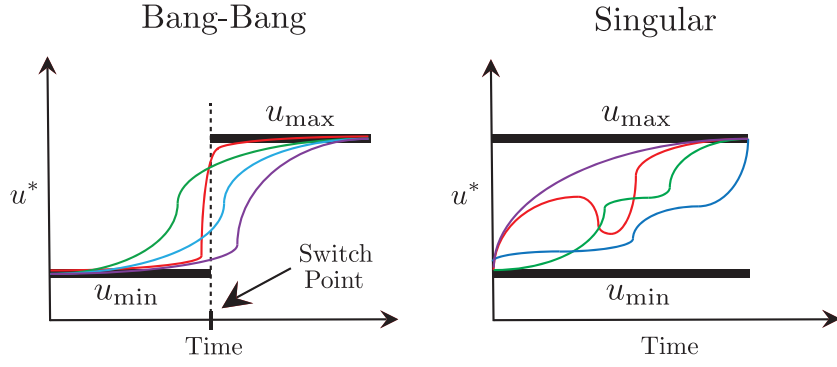


Figure 1: Numerical difficulties associated with bang-bang and singular control solutions.

control set will minimize the Hamiltonian. Furthermore, switching between nonsingular and singular arcs give rise to discontinuities on the state and control profiles, and the location of these transition points are referred to as *switch times*. The numerical challenges created by these discontinuities and non-uniqueness issues are illustrated in Fig. 1.

A common approach to determine unique singular controls over an arc is to repeatedly differentiate \mathcal{H}_u with respect to time until the control explicitly appears

$$\frac{d^{(r)}}{dt^{(r)}} \mathcal{H}_u = 0, \quad (r = 0, 1, 2, \dots). \quad (36)$$

An additional necessary condition for optimality is introduced to guarantee that the resulting singular control law is optimal. This condition is also referred to as the generalized Legendre-Clebsch condition [45, 49, 50],

$$(-1)^k \frac{\partial}{\partial u} \left[\frac{d^{2k}}{dt^{2k}} \mathcal{H}_u \right] \geq 0, \quad (k = 0, 1, 2, \dots), \quad (37)$$

where k represents the order of the singular arc. While in some problems of interest it is possible to use Eq. (36) to determine a condition for the singular control, in many cases it is unable to produce the singular control (for example, if the order of the singular arc is infinite). Even in cases where the singular control could be determined from Eq. (36), taking derivatives higher than second-order is not easy to implement numerically or algorithmically. As mentioned previously, the singular control might be a function of both the state and the costate. If this is the case then a direct collocation method could not be utilized to determine the optimal trajectory. In this paper a method is developed that can be fully automated for detecting and accurately approximating the solution of bang-bang and singular optimal control problems.

5 Method for Bang-Bang & Singular Optimal Control Problems

In this section the method for solving bang-bang and singular optimal control problems is developed. The method consists of two stages. The first stage of the method described in Section 5.1 details the detection of the control structure and the decomposition of the optimal control problem into a multiple-domain optimal control problem dictated by the discontinuities identified that are represented as domain interface variables. These domain interface variables are then treated as additional decision variables in the nonlinear programming problem (NLP). The first stage is only implemented on the first mesh iteration. The second stage described in Section 5.2 describes the new constraints that are added to the NLP depending on the structure detection's classification of a domain as being bang-bang or singular in order to constrain the modified optimal control problem correctly. The constraints and methods applied in each type of domain are provided in Section 5.2. The second stage initiates the iterative procedures in the proposed method described in Section 5.3.

5.1 Structure Detection and Decomposition

Assume now that the optimal control problem formulated in Section 2 under the assumptions of Section 4 has been transcribed into a NLP using multiple-domain LGR collocation developed in Section 3 with $D = 1$ (that is, a single domain is used). The solution obtained from the NLP then leads to estimates of the state, the control, and the costate as given in Eqs. (30) and (31), respectively. Assume further that the mesh refinement accuracy tolerance is not satisfied. As a result, mesh refinement is required which simultaneously enables the decomposition of the problem into domains that are either bang-bang, singular, or regular. This decomposition is obtained using structure detection as described now.

Structure detection locates discontinuities identified on the initial mesh and then uses the locations of the discontinuities to determine the classification of the interval formed by two adjacent discontinuities. In this work, only control discontinuities are considered because only problems where the Hamiltonian is linear in control are analyzed. Their locations are estimated using jump function approximations [19] and then the intervals formed by each discontinuity is analyzed using the switching function. Structure detection begins by applying the method of Section 5.1.1 to identify and estimate the locations of any control discontinuities. After discontinuity locations have been estimated, the method of Section 5.1.2

takes the estimated discontinuity locations and determines the classification of the domain as bang-bang or singular. The structure detection and decomposition process only occurs once on the initial solution. Detailed descriptions of the structure detection process are described next.

5.1.1 Identification of Control Switch Times

Discontinuities in each component of the control are identified using jump function approximations of the control solution as shown in Ref.[19]. In particular, the method given in Ref. [19] is employed here because it is effective for estimating locations of nonsmoothness in the optimal control. A brief overview of the process given in Ref. [19] is provided here for completeness. For further details related to jump function approximations for detecting nonsmoothness in an optimal control, see Ref. [19].

First, a jump function is defined as follows. Let $f : \mathbb{R} \rightarrow \mathbb{R}$ be an arbitrary function defined on the interval $t \in [t_0, t_f]$. The jump function of $f(t)$, denoted $[f](t)$, is defined as $[f](t) = f(t^+) - f(t^-)$ where $f(t^+)$ and $f(t^-)$ are the right-hand and left-hand limits of $f(t)$, $t \in [t_0, t_f]$. The jump function is zero across intervals where $f(t)$ is continuous and takes on the value of the jump in $f(t)$ at those locations where $f(t)$ is discontinuous. According to Ref. [19, 51] the jump function of a function $f(t)$ is approximated by

$$L_m f(t) = \frac{1}{q_m(t)} \sum_{t_j \in \mathcal{S}_t} c_j(t) f(t_j) \approx [f](t), \quad (38)$$

where $q_m(t)$ is defined by

$$q_m(t) = \sum_{t_j \in \mathcal{S}_t^+} c_j(t), \quad (39)$$

$c_j(t)$ is defined by

$$c_j(t) = \frac{m!}{\prod_{\substack{i=1 \\ i \neq j}}^{m+1} (t_j - t_i)}, \quad (40)$$

and m specifies the order of the approximation. Higher order approximations converge to the jump function faster outside the neighborhood of discontinuities but have oscillatory behavior in the vicinity of discontinuities. The oscillations are reduced via the **minmod** function, defined here as

$$MM(L_{\mathcal{M}} f(t)) = \begin{cases} \min_{m \in \mathcal{M}} L_m f(t), & L_m f(t) > 0 \quad \forall m \in \mathcal{M}, \\ \max_{m \in \mathcal{M}} L_m f(t), & L_m f(t) < 0 \quad \forall m \in \mathcal{M}, \\ 0 & \text{otherwise,} \end{cases} \quad (41)$$

where $\mathcal{M} \subset \mathbb{N}^+$ is a finite set of choices of the approximation order m .

Suppose an initial control solution is obtained. The control solution, $U(\tau_j^{(k)}), j = \{1, \dots, N_k\}; k = \{1, \dots, K\}$, is normalized to the interval $[0, 1]$ by the transformation

$$u(\tau_j^{(k)}) = \frac{U(\tau_j^{(k)}) - U_{\min}}{1 + U_{\max} - U_{\min}}, \quad (42)$$

where U_{\min} and U_{\max} are the minimum and maximum values of the control. Together, the normalized control solution and the corresponding collocation points, $\tau_j^{(k)}$ on $[-1, 1]$ of the initial mesh, are applied to Eqs. (38)–(41) to produce a jump function approximation for the normalized control. The jump function approximation is then evaluated at the points $\tau_{j+\frac{1}{2}}^{(k)} = \frac{1}{2}(\tau_j^{(k)} + \tau_{j+1}^{(k)}), j = \{1, \dots, N_k\}; k = \{1, \dots, K\}$. Let the evaluation of the jump function approximation at $\tau_{j+\frac{1}{2}}^{(k)}$ be denoted by $MM(\tau_{j+\frac{1}{2}}^{(k)})$. The method detects a discontinuity at the location, $\tau_{j+\frac{1}{2}}^{(k)}$, if the following condition is satisfied:

$$\left| MM(\tau_{j+\frac{1}{2}}^{(k)}) \right| \geq \eta. \quad (43)$$

The identified discontinuities are referred to as $b_i, i = \{1, \dots, n_d\}$ where n_d is the total number of identified control discontinuities. It is noted that $\eta \in [0, 1]$ in Eq. (43) is a user-specified threshold that specifies the relative size of jumps that are detected (where the likelihood of jumps being detected in the control decreases as η increases).

Bounds on the discontinuity locations are now defined. Consider for some $j = \{1, \dots, N_k\}$ and $k = \{1, \dots, K\}$ that Eq. (43) is satisfied, indicating that a discontinuity is present somewhere on the mesh interval $\tau \in [\tau_j^{(k)}, \tau_{j+1}^{(k)}]$. To account for the uncertainty incurred by using the numerical solution as a sample for the jump function approximation, a safety factor, $\mu \geq 1$ is introduced to extend the bounds estimated for the discontinuity. This safety factor provides a larger threshold to adequately capture the potential search space of the estimated switch times. Let $[b_i^-, b_i^+], i = \{1, \dots, n_d\}$ be the lower and upper bounds on the locations of discontinuities in the control (that is, any discontinuity is bounded to lie on the interval $[b_i^-, b_i^+]$).

The estimates of these bounds are defined as

$$\left. \begin{aligned} b_i^- &= \tau_{j+\frac{1}{2}}^{(k)} - \mu \left(\tau_{j+\frac{1}{2}}^{(k)} - \tau_j^{(k)} \right), \\ b_i^+ &= \tau_{j+\frac{1}{2}}^{(k)} + \mu \left(\tau_{j+1}^{(k)} - \tau_{j+\frac{1}{2}}^{(k)} \right), \end{aligned} \right\} \begin{aligned} i &= \{1, \dots, n_d\}, \\ j &= \{1, \dots, N_k\}, \\ k &= \{1, \dots, K\}. \end{aligned} \quad (44)$$

Larger values of μ are more desirable as it is more likely that the discontinuity b_i will lie in the interval $[b_i^-, b_i^+]$, $i = \{1, \dots, n_d\}$.

5.1.2 Identification of Bang-Bang and Singular Domains

Identification of the domains is employed to determine the structure of the control using the discontinuities identified from the jump function approximations. Specifically, the control solution is inspected to determine if any bang-bang or singular arcs exist. The first and second derivatives of the Hamiltonian with respect to control are computed and used to detect if the Hamiltonian is linear in the control by assessing if the second derivatives are zero. If the Hamiltonian is affine in control, the first derivatives are computed and represent the switching function of the system. If the Hamiltonian is not linear in the control the structure detection process is finished and smooth mesh refinement (see Section 5.2.4) can be performed.

Suppose the initial solution contains the following newly identified discontinuities b_i and corresponding bounds $[b_i^-, b_i^+]$, $i = \{1, \dots, n_d\}$. The solution is divided into intervals starting with the initial time, the discontinuity locations, and ending with the final time, $\{[-1, b_1], [b_1, b_i], \dots, [b_i, b_{i+1}], [b_{i+1}, +1]\}$, $i = \{1, \dots, n_d\}$. Next, the Hamiltonian in Eq. (33) is computed using the initial solution

$$\mathcal{H} = \mathbf{f}(\mathbf{X}(\tau), \boldsymbol{\lambda}(\tau)) + \phi^\top(\mathbf{X}(\tau), \boldsymbol{\lambda}(\tau))U(\tau) + \boldsymbol{\mu}^\top(\tau)\mathbf{c}(X(\tau), \tau). \quad (45)$$

Note that the costates are also obtained when solving the NLP that results from multiple-domain LGR collocation (see Section 3.1). The first and second derivatives with respect to the control are computed using the already computed derivatives required by the NLP solver

$$\frac{\partial \mathcal{H}}{\partial U} = \phi(\mathbf{X}(\tau), \boldsymbol{\lambda}(\tau), t(\tau, t_0, t_f)), \quad (46)$$

$$\frac{\partial^2 \mathcal{H}}{\partial U^2} = \Phi(\mathbf{X}(\tau), \boldsymbol{\lambda}(\tau), t(\tau, t_0, t_f)). \quad (47)$$

First, the values of Eq. (47) must be zero. If this condition is satisfied then Eq. (46) is analyzed as follows. A bang-bang interval in the control structure will occur when the switching function ϕ changes sign. The sign of the switching function ϕ is checked in each interval $[b_i, b_{i+1}]$, $i = \{1, \dots, n_d\}$. If the sign in the interval is positive, the control is constrained to its minimum value. If the sign in the interval is negative, the control is constrained to its maximum value. Additional details on these constraints are discussed in Section 5.2.1.

A singular interval in the control structure will occur when the switching function ϕ is zero at every

point in the interval $[b_i, b_{i+1}]$. Assessing if the switching function ϕ is zero over the current interval is not a trivial task. Due to the NLP being ill-conditioned when a singular arc is present, the estimated solution over a singular interval will suffer from larger numerical error. The user-defined zero threshold becomes critical in detecting the presence of a singular arc because the switching function will never be exactly zero. This threshold is heavily influenced by the coarseness of the initial mesh and the accuracy of the detected discontinuity locations. Once a singular arc has been detected, a regularization method is employed as described in Sections 5.2.2 and 5.2.3. If a scenario occurs where the entire control is singular on $[t_0, t_f]$, then no discontinuities will be detected. In this situation, the identification procedure is applied over the entire time domain so that the singular arc can be identified.

5.1.3 Structure Decomposition

Assuming the methods of Sections 5.1.1 and 5.1.2 have identified discontinuities and intervals that are bang-bang or singular, the initial mesh is now decomposed into the multiple-domain structure. Once acquired, the detected structure of the nonsmooth control is used to introduce the appropriate number of domain interface variables, $t_s^{[d]}$, $d = \{1, \dots, D-1\}$, to be solved for on subsequent mesh iterations, where the initial guess for each variable is the estimated discontinuity location b_i , $i = \{1, \dots, n_d\}$ that was found using the method in Section 5.1.1. The domain interface variables are included in the NLP by adding them as additional decision variables that define the new domains, $\mathcal{P}_d = [t_s^{[d-1]}, t_s^{[d]}]$, $d = \{1, \dots, D\}$. Specifically, the domain interface variables are employed by dividing the time horizon $t \in [t_0, t_f]$ of the original optimal control problem into D domains as described in Section 3.

Next, bounds on the domain interface variables are enforced to prevent the collapse or overlap of domains. The bounds provide an additional constraint on the domain interface variables. The upper and lower bounds on each domain interface variable are determined by taking the discontinuity bounds found in Section 5.1.1 and transforming them to the time interval $t \in [t_0, t_f]$ using the transformation in Eq. (15). Thus, the bounds $[b_i^-, b_i^+]$, $i = \{1, \dots, n_d\}$ are transformed to $[t_l^{[d-1]}, t_u^{[d]}]$, $d = \{1, \dots, D-1\}$.

This approach to structure decomposition partitions the entire problem domain into multiple domains of the form described in Section 3 such that the switch times are represented by the strategically placed domain interface variables $t_s^{[d]}$, $d \in \{1, \dots, D-1\}$. A schematic for the process of decomposing the nonsmooth control

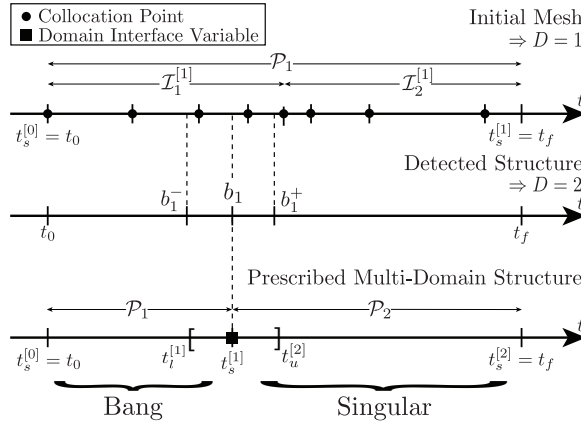


Figure 2: Schematic of process for decomposing the nonsmooth optimal control problem into D domains where the $D - 1$ domain interface variables are included as optimization variables to determine the optimal switch times in the control.

structure into a multiple-domain formulation with domain interface variables is shown in Fig. 2. Additionally, the form of the control in each domain is classified as either bang-bang, singular, or regular. In the next section, the constraints and refinement strategies required by each type of domain are discussed.

5.2 Domain Constraints and Refinement

Now that structure detection and decomposition has taken place by the methods of Section 5.1, additional constraints are required to properly constrain the multiple-domain optimal control problem. Recall that there are three types of domain classifications: bang-bang, singular, and regular. Each domain type requires its own set of constraints and refinement methods that are detailed in the following sections.

5.2.1 Bang-Bang Domain Constraints

Suppose the problem has been partitioned into D domains based on the results of structure detection, and it has been determined that \mathcal{B} domains are bang-bang by the method of Section 5.1.2, where $\mathcal{B} \leq D$. The value of the switching function ϕ in the current domain of interest \mathcal{P}_d is used to determine the value of the control over that domain. Recall, that the switching function assigns the value of the control according to

$$\begin{aligned} u^{[d]}(\tau) &= U_{\min} \quad , \quad \phi^{[d]}(\mathbf{X}, \boldsymbol{\lambda}, t(\tau, t_0, t_f)) > 0, \\ u^{[d]}(\tau) &= U_{\max} \quad , \quad \phi^{[d]}(\mathbf{X}, \boldsymbol{\lambda}, t(\tau, t_0, t_f)) < 0. \end{aligned} \tag{48}$$

The control is then constrained to its corresponding maximum or minimum value in the resulting multiple-domain optimal control problem. The bang-bang control is now appropriately constrained over its domain and the corresponding domain interface variables can be optimized to the optimal switch time locations.

5.2.2 Regularization of a Singular Domain

Assume now that the entire domain $[t_0, t_f]$ of the optimal control problem has been partitioned into D domains using the structure detection method as described in Section 5.1. Assume further that, using the procedure given in Section 5.1.2, \mathcal{S} of these D domains are classified as singular (where $\mathcal{S} \leq D$ and $\mathcal{S} + \mathcal{B} \leq D$) such that $\{s_1, \dots, s_{\mathcal{S}}\} \subseteq \{1, \dots, D\}$ are the indices corresponding to the singular domains. The singular domains are then defined, respectively, on the intervals $[t_s^{[s_d-1]}, t_s^{[s_d]}] \subseteq [t_0, t_f]$, $d = \{1, \dots, \mathcal{S}\}$.

In any domain that is classified as singular, the following iterative regularization method is employed. First, the objective functional in the singular domain is augmented with the regularization term

$$\delta_{s_d} = \frac{\epsilon}{2} \int_{t_s^{[s_d-1]}}^{t_s^{[s_d]}} (u(t) - \alpha_p(t))^2 dt, \quad d = \{1, \dots, \mathcal{S}\}, \quad (49)$$

where $u(t)$ is the optimal control to be determined when solving the problem, $\alpha_p(t) \in \mathbb{R}$ is a known function that changes with each iteration of the regularization method (see Section 5.2.3), and

$$\frac{\epsilon}{2} (u(t) - \alpha_p(t))^2 \quad (50)$$

is the integrand of Eq. (49). Furthermore, ϵ is a user-defined weighting parameter that is chosen based on the particular problem under consideration. Augmenting the Hamiltonian with the term in Eq. (50) results in a Hamiltonian that is quadratic in the control. Consequently, the optimal control problem, that would be singular without the inclusion of the term in Eq. (50), becomes regular (nonsingular). While in principle ϵ can be any positive value, it must be sufficiently large to eliminate the indeterminacy of determining the optimal control on the singular arc, but it must be sufficiently small so that the resulting optimal control is in close proximity to the true singular optimal control.

5.2.3 Iterative Procedure for Determining Singular Control

Next, it is important to understand the source of the function $\alpha_p(t)$. Singular domain refinement is employed in an iterative fashion where p is the iteration number of the singular domain refinement procedure. For $p = 1$,

$\alpha_p(t)$ is set to zero. Then, for $p > 1$, $\alpha_p(t)$ is obtained using a continuous piecewise cubic approximation of the control obtained from the solution of the NLP on iteration $p - 1$ and the approximation for $\alpha_p(t)$ is obtained in a manner described in Ref. [52].

The augmented multiple-domain optimal control problem that is solved by the regularization method is then stated as follows. First, for any iteration $p \geq 1$ the objective functional to be minimized includes the terms δ_{s_d} , $\{d = 1, \dots, S\}$, and is defined as

$$\mathcal{J}_a = \mathcal{J} + \sum_{d=1}^S \delta_{s_d}. \quad (51)$$

Furthermore, the constraints include the dynamic constraints, the boundary conditions, and the path constraints given, respectively, in Eqs. (2)–(5). The process for updating the iteration of the regularization method is as follows. First, after solving the NLP arising from LGR collocation with $D = 1$, the structure detection and decomposition method of Section 5.1 is employed for one mesh iteration. On the second mesh iteration (that is, $M = 2$) the value of p is set to unity (that is, $p \equiv 1$) and the regularization term of Eq. (49) is augmented to the objective functional in any domain classified as singular with $\alpha_p(t) \equiv 0$ and the resulting NLP is then solved. Then, from the third mesh iteration onwards (that is, $M > 2$), the value of p is incremented as $p \rightarrow p + 1$ and the value of $\alpha_p(t)$ is determined based on the aforementioned continuous piecewise cubic approximation from the discrete control solution obtained on iteration p . The process of refining the mesh and updating the function $\alpha_p(t)$ is then repeated until the regularization term δ lies below a user-specified tolerance σ . The regularization procedure is independent of regular mesh refinement meaning that refinement of the mesh always occurs on each iteration and the updates to $\alpha_p(t)$ occur independently from the mesh refinement actions. Figure 3 provides a schematic of the regularization method that is enforced over each mesh refinement iteration in a singular domain.

Now, it has been shown that as $p \rightarrow \infty$ the solution of the augmented problem in Eqs. (2)–(5) and (51) approaches the singular solution of the original optimal control problem [34]. Note, however, that while a key goal of the regularization method is to *reduce* the difference between the singular control $u(t)$ and the approximated control $\alpha_p(t)$ in the regularization term of Eq. (49), the goal is *not* to drive the difference between $u(t)$ and $\alpha_p(t)$ to exactly zero. In fact, maintaining a nonzero difference between $u(t)$ and $\alpha_p(t)$ is critical because, if the difference between $u(t)$ and $\alpha_p(t)$ is exactly zero, the regularization term δ_{s_d} , $d = \{1, \dots, S\}$ is itself zero and the solution of the optimal control problem reverts to being singular. Thus, the

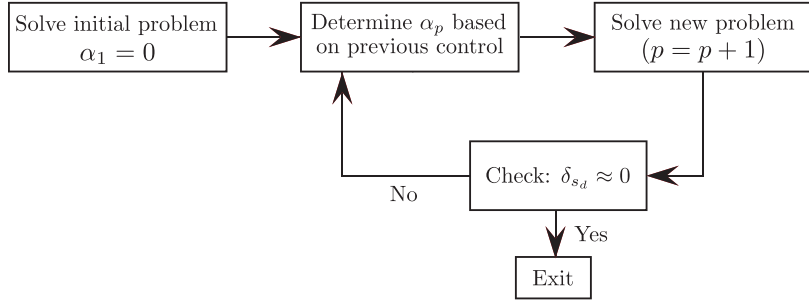


Figure 3: Description of the regularization method during mesh refinement iteration, M .

goal is to make the regularization term large enough so that the solution remains nonsingular (thus, avoiding numerical difficulties associated with a singular control) but to make the regularization term small enough to obtain a control that lies in close proximity to the singular control.

5.2.4 Regular Domain Refinement

Suppose that a particular domain \mathcal{P}_d has been determined to be regular, that is, the domain \mathcal{P}_d is categorized neither as bang-bang nor singular. Although the domain \mathcal{P}_d is categorized as regular, this domain may still require mesh refinement. In particular, mesh refinement of the domain \mathcal{P}_d will be required if the maximum relative error on the domain \mathcal{P}_d exceeds the relative error tolerance. Several methods have been previously developed for smooth mesh refinement [10, 17, 20, 21]. In this research, domains where the solution is smooth are refined using the method developed in Ref. [10]. The mesh refinement method of Ref [10] occurs on every iteration until the user-specified mesh error tolerance is met and is independent of the status of the regularization procedure in Section 5.2.2. It is noted that Ref. [10] also includes a method for the computation of a relative error estimate. The reader is referred to Ref. [10] for a more detailed explanation of how both smooth mesh refinement operates and an estimate of the relative error on a mesh.

5.3 Procedure for Solving Bang-Bang and Singular Optimal Control Problems

An overview of the proposed method for bang-bang and singular optimal control problems is shown below. The mesh refinement iteration is denoted by M and is incremented by one with each loop of the method. The regularization refinement iteration is denoted by p and is incremented by one on each mesh iteration

as required by the regularization method. This method terminates when two requirements are met. First, the regularization term (49) must be within a user specified tolerance σ from zero, or if Eq. (49) remains identical in value over three consecutive iterations. Second, the mesh error tolerance, e , must be satisfied on each mesh interval or if M reaches a prescribed limit, M_{\max} . The method is executed as follows:

Method for Solving Bang-Bang & Singular Optimal Control Problems

Step 1: Set $M = 0$ and specify initial mesh. All mesh intervals form a single domain.

Step 2: Solve NLP of Section 3 on mesh M .

Step 3: If $M = 1$, employ structure detection and decomposition in Section 5.1.

- (a): Determine the number of switch times, n_d , using the methods of Section 5.1.1.
- (b): Classify the intervals as bang-bang or singular using the method of 5.1.2.
- (c): Assign domain interface variables by method of Section 5.1.3.
- (d): Partition time horizon into domains by method of Section 5.1.3.
- (e): Perform domain refinement according to Section 5.2.
 - (i): Enforce control constraints in each bang-bang domain as in Section 5.2.1.
 - (ii): Employ regularization method in singular domains according to Section 5.2.2.
 - (iii): Apply mesh refinement in regular domains as in Section 5.2.4.

Step 4: If $n_d = 0$ or $M > 1$, apply smooth mesh refinement and proceed to **Step 7**.

Step 5: Compute relative error e on current mesh M .

Step 6: If $M > 1$, $\delta \leq \sigma$, and $e_{\max} \leq e$ or $M > M_{\max}$, then quit. Otherwise:

- (a): Apply iterative procedure of Section 5.2.3.
- (b): Increment $M \rightarrow M + 1$, $p \rightarrow p + 1$ and return to **Step 2**

Step 7: Increment $M \rightarrow M + 1$ and return to **Step 2**.

6 Examples

In this section, four nontrivial bang-bang and singular optimal control problems are solved using the method described in Section 5. Each of the four problems demonstrates the methods abilities to solve different types of nonsmooth optimal control problems including a purely bang-bang control, a bang-singular-bang control with no analytic solution, a bang-singular control where the analytic solution exists, and finally a problem with both a finite and infinite-order singular arc as well as bang-bang arcs across multiple control components. A fifth example with a smooth optimal solution is also solved using the method of Section 5 and compared against a previously developed mesh refinement method.

The following conventions are used for all of the examples. The proposed method for solving bang-bang and singular optimal control problems developed in Section 5 is referred to as the BBSOC method. The example problems are also solved using `GPOPS-III` [53] in `MATLAB` for comparison. Furthermore, the BBSOC method is validated for each example using either the analytic solution, if it exists, or a *baseline* solution obtained using the optimality conditions presented in Section 2. All results are obtained using `MATLAB` and the nonlinear program developed in Section 3 is solved using IPOPT [2] in full-Newton mode. The NLP solver tolerance is set to 10^{-8} and the mesh refinement tolerance for smooth mesh refinement [53]) is set to 10^{-6} . All first and second derivatives are supplied to IPOPT using the automatic differentiation software ADiGator [54]. In each example, the initial mesh consists of ten uniformly spaced mesh intervals and four collocation points per mesh interval, and the initial guess for all examples is a straight line for variables with boundary conditions at both endpoints and is a constant for variables with boundary conditions at only one endpoint. Finally, all computations were performed on a 2.9 GHz 6-Core Intel Core i9 MacBook Pro running Mac OS Big Sur Version 11.3 with 32 GB 2400 MHz DDR4 of RAM, using `MATLAB` version R2019b (build 9.7.0.1190202) and all computation (CPU) times are in reference to this aforementioned machine.

Example 1: Robot Arm Problem

Consider the following problem where the goal is to reorient a robotic arm in minimum time [55]:

$$\begin{aligned}
 & \text{minimize} \quad \mathcal{J} = t_f, \\
 & \text{subject to} \quad \left\{ \begin{array}{lll}
 y_1(t) = y_2(t) & , & y_1(0) = 9/2 \quad , \quad y_1(t_f) = 9/2, \\
 \dot{y}_2(t) = u_1(t)/L & , & y_2(0) = 0 \quad , \quad y_2(t_f) = 0, \\
 \dot{y}_3(t) = y_4(t) & , & y_3(0) = 0 \quad , \quad y_3(t_f) = 2\pi/3, \\
 \dot{y}_4(t) = u_2(t)/I_\theta & , & y_4(0) = 0 \quad , \quad y_4(t_f) = 0, \\
 \dot{y}_5(t) = y_6(t) & , & y_5(0) = \pi/4 \quad , \quad y_5(t_f) = \pi/4, \\
 \dot{y}_6(t) = u_3(t)/I_\phi & , & y_6(0) = 0 \quad , \quad y_6(t_f) = 0, \\
 -1 \leq u_i(t) \leq 1, \quad (i = 1, 2, 3) \quad ,
 \end{array} \right. \quad (52)
 \end{aligned}$$

where t_f is free, $I_\phi = \frac{1}{3}((L - y_1(t))^3 + y_1^3(t))$, $I_\theta = I_\phi \sin^2(y_5(t))$, and $L = 5$. The robot arm problem has a bang-bang structure for all three components of the control components and contains a total of five discontinuities in the control. Given that the dynamics in Eq. (52) cannot be solved analytically but the optimal control is known to be piecewise constant, it is possible to use the known optimal control structure to compute a highly accurate approximation of the solution to this example by dividing the problem into six phases such that each control component is fixed in each phase at either its lower or upper limit and introduce variables that define the times at which a control component switches from one value to another. This numerical approximation is referred to as a *baseline* solution and is, for all practical purposes, considered exact (even though, strictly speaking, it is not exact). The switch times and the optimal objective obtained using the aforementioned six-phase formulation with the optimal control software **GPOPS – III** [53] is shown in Table 1.

The control solution obtained from solving this problem using the BBSOC method and **GPOPS – III** are shown in Fig. 4. Observing the controls in Figs. 4a–4c, it is seen that the five switch times are identified and the controls are constrained to their corresponding boundaries after just one iteration of the BBSOC method. In contrast, **GPOPS – III** does not correctly identify all five discontinuities and as a result obtains incorrect approximations of the controls. The method of **GPOPS – III** attempts to place more collocation points surrounding the switch times resulting in a higher dimensional problem that still fails to identify the

Table 1: Comparison of computational results for Example 1.

	$t_s^{[1]}$	$t_s^{[2]}$	$t_s^{[3]}$	$t_s^{[4]}$	$t_s^{[5]}$	\mathcal{J}^*	CPU [s]
BBSOC	2.285228	2.796043	4.570456	6.344869	6.855684	9.140912	0.63
GPOPS – III	2.249813	2.795031	4.518293	6.330691	6.820305	9.140984	3.25
Baseline	2.285228	2.796043	4.570456	6.344869	6.855684	9.140912	1.59

exact locations of the control switches. Table 1 shows the numerical values of the switch times obtained using the BBSOC method, GPOPS – III, and the baseline method. It is seen that the BBSOC method produces highly accurate approximations of both the switch times and objective and is in excellent agreement with the baseline solution. On the other hand, GPOPS – III, which is not designed specifically for solving problems with nonsmooth solutions, attains a much less accurate solution when compared with the BBSOC method. In addition to accuracy, Table 1 provides a comparison of the CPU time required for each approach. In particular, it is seen from Table 1 that the BBSOC method converges to the optimal solution more efficiently compared with either GPOPS – III or the baseline solution. Next, Fig. 4d shows the switching functions that correspond to each of the control components. Again, it is seen that the switching functions identify accurately the multiple-switching structure of the optimal control.

Example 2: Goddard Rocket Problem

Consider the following optimal control problem [45]:

$$\begin{aligned}
 & \text{maximize} \quad \mathcal{J} = h(t_f), \\
 & \text{subject to} \quad \begin{cases} \dot{h}(t) = v(t) & , \quad h(0) = 0 \quad , \quad h(t_f) = \text{Free}, \\ \dot{v}(t) = \frac{T(t)-D}{m(t)} - g & , \quad v(0) = 0 \quad , \quad v(t_f) = \text{Free}, \\ \dot{m}(t) = -\frac{T(t)}{c} & , \quad m(0) = 3 \quad , \quad m(t_f) = 1, \\ 0 \leq T(t) \leq T_{\max} & , \end{cases} \end{aligned} \tag{53}$$

where h is the altitude, v is the velocity, m is the mass, T is the thrust (and is the control), $D = D_0 v^2(t) \exp(-h(t)/H)$, and the final time is free. Further details on the model and the parameters can be found in Ref. [45]. In particular, the control T has a bang-singular-bang structure and differentiating \mathcal{H}_u

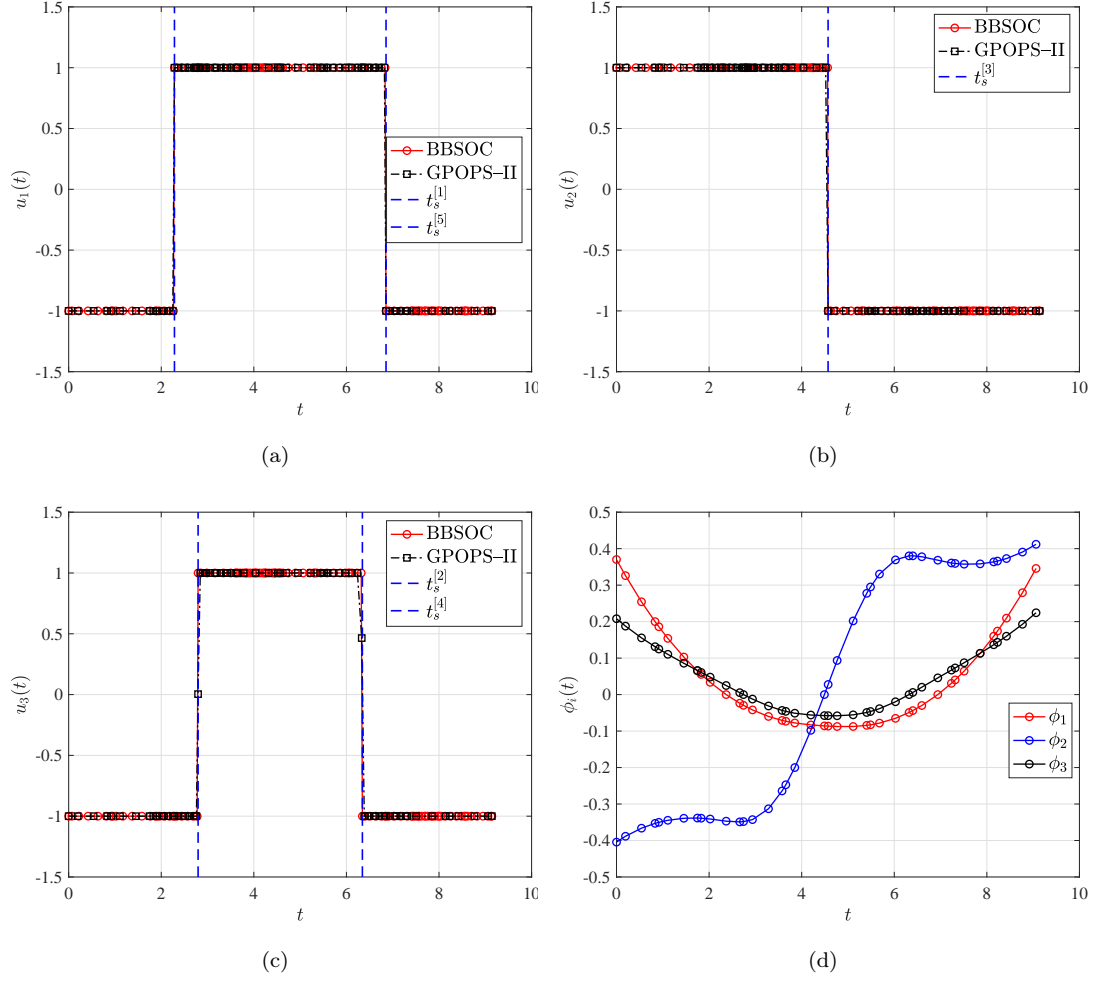


Figure 4: Control component solutions for Example 1 and the corresponding switching functions obtained by the BBSOC method and GPOPS – II.

twice with respect to time leads to the following singular control law [1]:

$$T_{\text{sing}}(t) = D + m(t)g + \left[\frac{c^2(1 + \frac{v(t)}{c})}{Hg} - 1 - \frac{2c}{v(t)} \right] \left[\frac{m(t)g}{1 + \frac{4c}{v(t)} + \frac{2c^2}{v^2(t)}} \right]. \quad (54)$$

Given that the dynamics in Eq. (53) cannot be solved analytically but the optimal control is known to be piecewise continuous, it is possible to use the known optimal control structure to compute a highly accurate approximation of the solution to this example by dividing the problem into three phases such that the control is fixed in each phase at either its lower limit, upper limit, or with Eq. (54) enforced as a path constraint and introduce variables that define the times at which a control component switches from one value to another. This numerical approximation is referred to as a *baseline* solution and is, for all practical purposes, considered exact (even though, strictly speaking, it is not exact). The switch times and the optimal objective obtained using the aforementioned three-phase formulation with the optimal control software `GPOPS-III` [53] are shown in Table 2.

The problem in Eq. (53) is solved using the BBSOC method and `GPOPS-III`. Both of these control solutions are compared in Fig. 5a and parameters related to the regularization method are provided in Table 2. Figure 5a demonstrates that the regularization method has converged to the correct singular control while also correctly identifying the switch times. In contrast, `GPOPS-III` obtains a solution that exhibits oscillations at the switch times defining the singular arc. These oscillations are also seen in the initial iterations of the regularization method, but are removed by the third iteration as seen in Fig. 5b.

Next, Table 2 compares the solution obtained using the BBSOC method, `GPOPS-III`, and the baseline solution. These results further validate the BBSOC methods ability to identify the optimal switch times, final time, and cost. The BBSOC results are also in close agreement with the baseline solution. In contrast, the `GPOPS-III` results are not in agreement with the baseline solution. The computation times for all three methods are also compared in Table 2 and all three methods have very similar CPU times with the BBSOC method taking the longest, but it produces a far more accurate solution and achieves the same accuracy as the baseline solution without any a priori knowledge of the singular problem. Finally, Fig. 5c shows the switching function that corresponds to the control. This switching function is obtained using the initial control solution and is used to identify the boundary that the control should be constrained to in each domain. The switching function is also provided in Fig. 5c to show when the function switches from positive values to zero, indicating a singular arc is present.

Table 2: Comparison of computational results for Example 2.

	$t_s^{[1]}$	$t_s^{[2]}$	t_f	\mathcal{J}^*	δ	ϵ	p	CPU [s]
BBSOC	13.751266	21.987362	42.887912	18550.87185	7.86×10^{-8}	10^{-6}	3	2.86
GPOPS – III	13.541287	22.213037	42.887750	18550.87039	–	–	–	2.24
Baseline	13.751270	21.987363	42.887912	18550.87186	–	–	–	2.57

It is known that the singular surface in the optimal control problem of Eq. (53) can be reduced to lie in the state space (that is, the singular surface is a three-dimensional surface in the space defined by h , v , and m). In particular, the singular surface is defined as

$$m = \frac{D_0 v^2 \exp(-h/H)(1 + v/c)}{g}. \quad (55)$$

Figure 6 shows the singular surface defined by Eq. (55) and the state solution obtained using the BBSOC method, GPOPS – III, and baseline method. It is observed in Fig. 6b that the solution obtained using GPOPS – III that should correspond to the singular interval does not lie in close proximity to the singular surface. On the other hand, the portion of the trajectory corresponding to the singular interval using either the BBSOC or the baseline method does lie in close proximity to the singular surface.

Example 3: Aly Problem

Consider the following linear-quadratic regulator problem presented in [56]:

$$\begin{aligned} \text{minimize} \quad & \mathcal{J} = \frac{1}{2} \int_0^{t_f} (x_1^2(t) + x_2^2(t)) dt, \\ \text{subject to} \quad & \begin{cases} \dot{x}_1(t) = x_2(t) & , \quad x_1(0) = 0 & , \quad x_1(t_f) = \text{Free}, \\ \dot{x}_2(t) = u(t) & , \quad x_2(0) = 1 & , \quad x_2(t_f) = \text{Free}, \\ -1 \leq u(t) \leq 1 & , \end{cases} \end{aligned} \quad (56)$$

where $t_f = 5$. The optimal control problem of Eq. (56) has an analytic solution. Consequently, the analytic solution can be used to assess the accuracy of the BBSOC method. Further details on the derivation of the analytic solution to the example in Eq. (56) can be found in [56]. The singular control is $u_{\text{sing}}^*(t) = x_1(t)$, $t \geq \approx 1.41376409$ and the analytic switch time $t_s^{[1]} = 1.41376409$ is shown in Table 3.

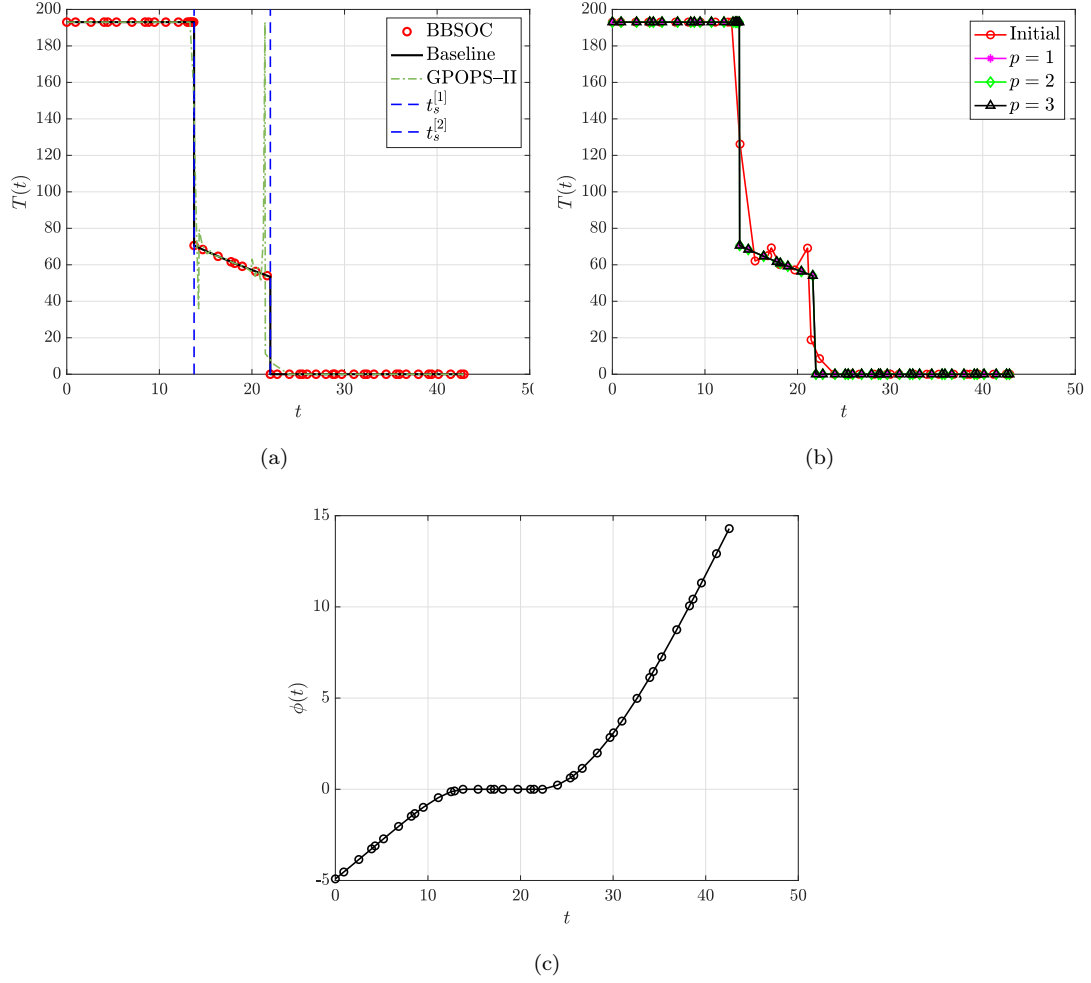


Figure 5: Control solution for Example 2 and the corresponding switching function obtained by the BBSOC method, GPOPS – II, and the baseline method.

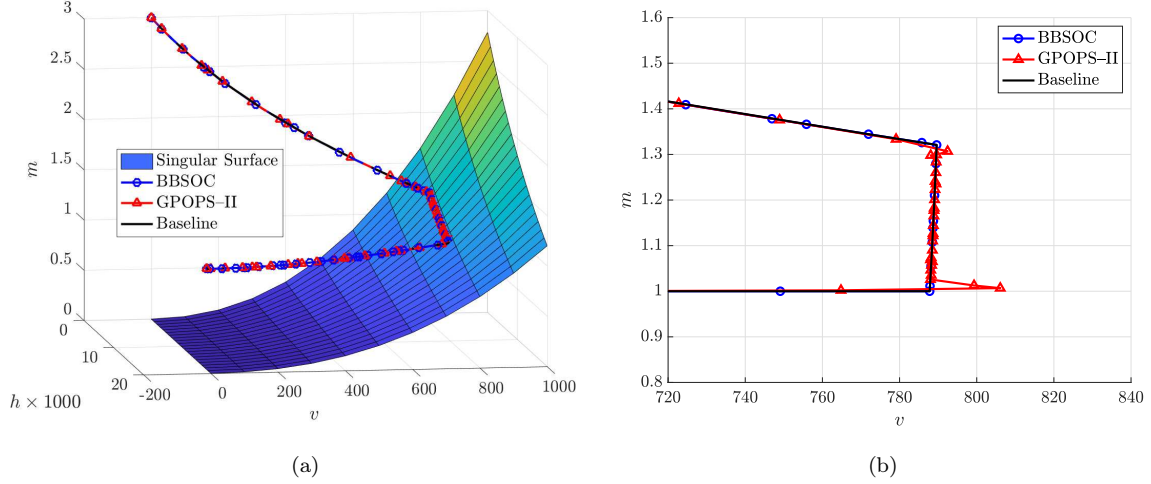


Figure 6: The singular surface for Example 2 is presented with the corresponding trajectory obtained using the BBSOC method, $\mathbb{GPOPS} - \text{III}$, and the baseline method.

Figure 7 shows the control solutions obtained when solving the optimal control problem of Eq. (56) using both the BBSOC method and $\mathbb{GPOPS} - \text{III}$. Using the BBSOC method, it is seen that a high-accuracy approximation of both the switch time and the singular control are obtained after two iterations of the BBSOC method. In contrast, the solution obtained using $\mathbb{GPOPS} - \text{III}$ exhibits fluctuations in the neighborhood of the switch time. Next, Fig. 7b shows the history of the control obtained on each iteration of the regularization method that is part of the BBSOC method. As already indicated in Fig. 7 and further emphasized by Fig. 7b, these fluctuations present in the $\mathbb{GPOPS} - \text{III}$ solution are eliminated because of the inclusion of the regularization term in the objective functional.

Next, Table 3 provides a comparison of the switch time and objective values obtained using both the BBSOC method and $\mathbb{GPOPS} - \text{III}$ alongside the analytic solution (where it is noted that Table 3 also provides the parameter ϵ used in the regularization term of Eq. (49) along with the value δ obtained for the regularization term itself). It is seen that the value of the analytic switch time is in close agreement with the switch time obtained from the BBSOC method. Next, the computation times for both methods are also compared in Table 3. It is observed that the BBSOC method is more computationally efficient when compared with $\mathbb{GPOPS} - \text{III}$ while simultaneously producing a more accurate solution. Finally, Fig. 7c shows the switching function. It is seen in Fig. 7c that the switching function changes from positive to zero, indicating

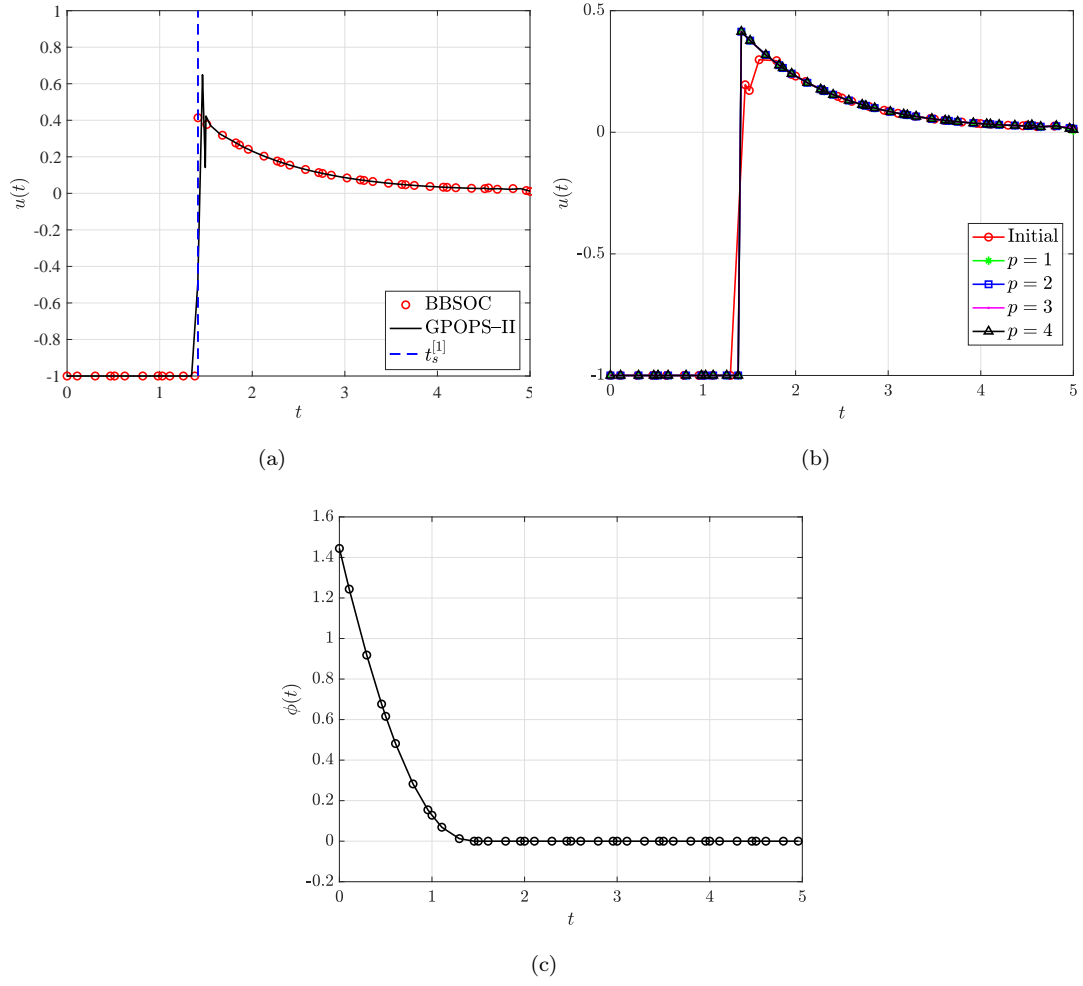


Figure 7: Control solution for Example 3 and the corresponding switching function obtained by the BBSOC method and GPOPS – III.

the presence of a singular arc in the solution.

Table 3: Comparison of computational results for Example 3

	$t_s^{[1]}$	\mathcal{J}^*	δ	ϵ	p	CPU [s]
BBSOC	1.41376404	0.37699193	6.31×10^{-14}	10^{-8}	4	2.02
GPOPS – III	1.41194167	0.37699503	–	–	–	2.13
Analytic	1.41376409	–	–	–	–	–

Example 4: Minimum Time Reorientation of a Spacecraft

Consider the following minimum-time rigid body reorientation optimal control problem [57]:

$$\begin{aligned}
 & \text{minimize} \quad \mathcal{J} = t_f, \\
 & \text{subject to} \quad \left\{ \begin{array}{l}
 \dot{\omega}_1(t) = a\omega_{30}\omega_2(t) + u_1(t), \\
 \dot{\omega}_2(t) = -a\omega_{30}\omega_1(t) + u_2(t), \\
 \dot{x}_1(t) = \omega_{30}x_2(t) + \omega_2(t)x_1(t)x_2(t) + \frac{\omega_1(t)}{2}(1 + x_1^2(t) - x_2^2(t)), \\
 \dot{x}_2(t) = \omega_{30}x_1(t) + \omega_1(t)x_1(t)x_2(t) + \frac{\omega_2(t)}{2}(1 + x_2^2(t) - x_1^2(t)), \\
 \omega_1(0) = \omega_{10}, \quad \omega_1(t_f) = \omega_{1f}, \\
 \omega_2(0) = \omega_{20}, \quad \omega_2(t_f) = \omega_{2f}, \\
 x_1(0) = x_{10}, \quad x_1(t_f) = x_{1f}, \\
 x_2(0) = x_{20}, \quad x_2(t_f) = x_{2f}, \\
 |u_i| \leq u_{i,\max}(t), \quad i = 1, 2,
 \end{array} \right. \quad (57)
 \end{aligned}$$

where $\omega_i(t)$ is the angular velocity, $x_i(t)$ is the position of the spacecraft, ω_{30} is the initial condition for $\omega_3(t)$ which remains constant, and $u_{i,\max} = 1$. For the purposes of demonstrating the capabilities of the BBSOC method, two special cases of the optimal control problem given in Eq. (57) will be analyzed. These two cases are those of a nonspinning axisymmetric rigid body and the an inertially symmetric rigid body. It is known for Case 1 that a portion of the optimal solution lies on a second-order singular arc whereas for Case 2 the solution lies on an infinite-order singular arc. For further details of the analysis of the singular controls for these two cases see Ref. [57].

Case 1: Nonspinning Axisymmetric Rigid Body: $(a, \omega_{30}) = (0.5, 0)$

For the case $(a, \omega_{30}) = (0.5, 0)$ and the boundary conditions

$$\begin{aligned}\omega_{10} &= -0.45 & , & \quad \omega_{1f} = 0, \\ \omega_{20} &= -1.1 & , & \quad \omega_{2f} = 0, \\ x_{10} &= 0.1 & , & \quad x_{1f} = 0, \\ x_{20} &= -0.1 & , & \quad x_{2f} = 0,\end{aligned}$$

a portion of the optimal solution lies on a second-order singular arc [57]. In particular, the control u_1 has a bang-singular structure while the control u_2 is bang-bang (that is, u_2 is not singular). More specifically, the singular optimal control is $u_{1,\text{sing}}^*(t) = 0$ [57]. Given that the dynamics in Eq. (57) cannot be solved analytically but the optimal control is known to be piecewise constant, it is possible to use the known optimal control structure to compute a highly accurate approximation of the solution to this example by dividing the problem into six phases such that each control component is fixed in each phase at either its lower limit, upper limit, or singular value, and introduce variables that define the times at which a control component switches from one value to another. This numerical approximation is referred to as a *baseline* solution and is, for all practical purposes, considered exact (even though, strictly speaking, it is not exact). The switch times and the optimal objective obtained using the aforementioned six-phase formulation with the optimal control software **GPOPS – III** [53] is shown in Table 4.

The control solutions obtained using the BBSOC method and **GPOPS – III** are shown in Fig. 8, where it is seen that the BBSOC solution is in close agreement with the baseline solution. In particular, Fig. 8a shows that the singular control u_1 obtained using the BBSOC method is approximated to a high accuracy and the five switch times are identified using the BBSOC method. In contrast, **GPOPS – III** obtains a control solution that exhibits oscillatory behavior due to the ill-conditioning of the NLP. Figure 8e shows each control solution at every iteration of the regularization procedure to show how the BBSOC method efficiently eliminates the oscillations in the initial control solution.

Next, Table 4 provides the switch time locations and final time obtained by each of the three methods along with the parameters required for the regularization method. While the switch times obtained by each method seem to be in excellent agreement, the actual control profiles obtained are not as explained previously. Finally, Figs. 8c and 8d show the switching functions that correspond to each of the control components.

Table 4: Comparison of computational results for Case 1 of Example 4.

	$t_s^{[1]}$	$t_s^{[2]}$	$t_s^{[3]}$	$t_s^{[4]}$	$t_s^{[5]}$	\mathcal{J}^*	δ	ϵ	p	CPU [s]
BBSOC	0.6498	1.2898	1.8188	1.9084	1.9919	2.8839	1.24×10^{-10}	10^{-3}	2	3.37
GPOPS – III	0.6498	1.2897	1.8184	1.9226	1.9922	2.8839	–	–	–	5.18
Baseline	0.6498	1.2898	1.8177	1.9054	1.9919	2.8839	–	–	–	0.42

The switching functions are obtained using the initial control solution and are used to identify the boundary that the control should be constrained to in each domain. The switching functions also indicate the presence of bang-bang arcs and a singular arc in the controls. Finally, the computation times for all three solutions are also shown in Table 4. It is seen that the BBSOC method obtains a solution with greater computational efficiency than GPOPS – III, but obtains a solution with lower computational efficiency compared with the baseline solution.

Case 2: Inertially Symmetric Rigid Body: $(a, \omega_{30}) = (0, -0.3)$

For the case $(a, \omega_{30}) = (0, -0.3)$ and the boundary conditions

$$\begin{aligned}
 \omega_{10} &= 0 \quad , \quad \omega_{1f} = 1, \\
 \omega_{20} &= 0 \quad , \quad \omega_{2f} = 2, \\
 x_{10} &= 0 \quad , \quad x_{1f} = \text{Free}, \\
 x_{20} &= 0 \quad , \quad x_{2f} = \text{Free},
 \end{aligned}$$

the optimal solution lies on an infinite-order singular arc [57]. In particular, the control u_1 is totally singular while the control u_2 is bang (that is, u_2 is not singular). More specifically, one possible solution to the singular optimal control is $u_{1,\text{sing}}^*(t) = 0.5$ [57]. Given that the dynamics in Eq. (57) cannot be solved analytically but the optimal control is known to be constant (for this one particular solution), it is possible to use the known optimal control structure to compute a highly accurate approximation of the solution to this example by fixing each control component at either its lower limit, upper limit, or singular value. This numerical approximation is referred to as a *baseline* solution and is, for all practical purposes, considered exact (even though, strictly speaking, it is not exact). The optimal objective obtained using the aforementioned formulation with the optimal control software GPOPS – III [53] is shown in Table 5.

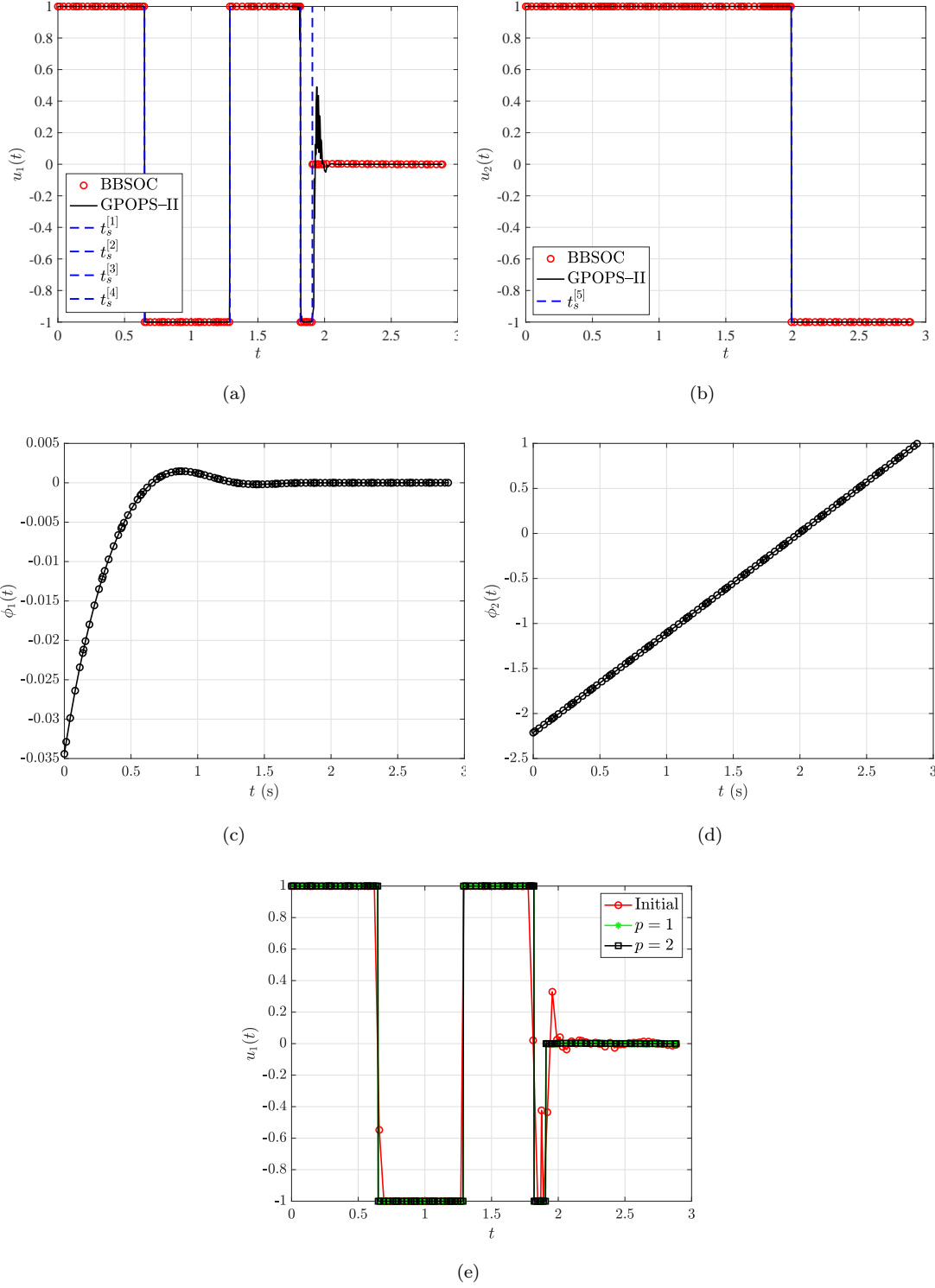


Figure 8: Control component solutions for Case 1 of Example 4 and the corresponding switching function obtained by the BBSOC method and GPOPS – II.

Table 5: Comparison of computational results for Case 2 of Example 4.

	\mathcal{J}^*	δ	ϵ	p	CPU [s]
BBSOC	2.00	1.11×10^{-19}	10^{-1}	2	3.18
GPOPS – III	2.00	–	–	–	1.63
Baseline	2.00	–	–	–	0.51

For Case 2, the entire time domain is singular and the problem does not need to be divided into domains. As a result the BBSOC method does not assign any domain interface variables and instead the regularization method is applied over the entire, single time domain. Table 5 provides the optimal objective obtained using the BBSOC method, GPOPS – III, and the baseline solution. It appears that all three solutions are in agreement; however, it can be seen in Fig. 9a that the control obtained using GPOPS – III is actually incorrect. In Fig. 9c, the regularization method converges to the optimal singular control whereas the GPOPS – III solution exhibits highly oscillatory behavior due to the ill-conditioning of the NLP. The same observations are also made for the second bang-bang control component in Fig. 9b. The computation times for all three methods are also compared in Table 5. The BBSOC converges to a higher accuracy solution than GPOPS – III, but at the cost of an increased computation time. The switching functions are also provided in Fig. 9d to show that the function remains constant at either zero or a negative value, indicating the presence of singular arcs and bang-bang arcs. Case 2 illustrates the BBSOC methods ability to detect and approximate infinite-order singular controls to a high accuracy.

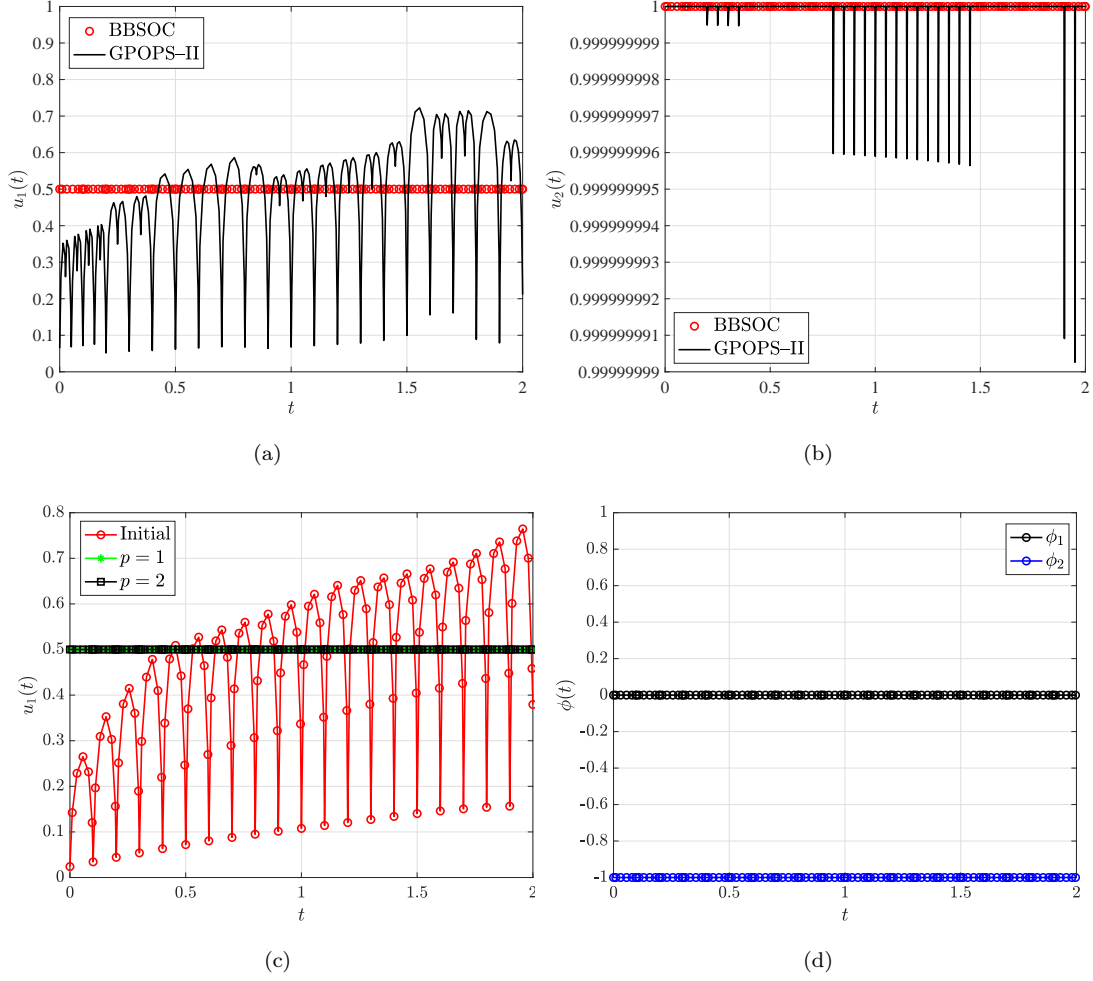


Figure 9: Control component solutions for Case 2 of Example 4 and the corresponding switching function obtained by the BBSOC method and GPOPS – II.

Example 5: Entry Vehicle Crossrange Maximization (Smooth Solution)

Consider now the crossrange maximization of an entry vehicle problem given in Ref. [1] and whose formulation is taken from Ref. [53]. It is known that the solution to this optimal control problem is smooth. For problems whose solutions are smooth, the BBSOC method should not identify any discontinuities or singular intervals. Consequently, the method should not divide the entire domain into multiple domains nor should it apply regularization. In this section the entry vehicle problem is solved using the BBSOC method. While the details of this problem are omitted here for brevity, further details of the maximum crossrange entry vehicle problem can be found in Ref. [1, 53].

The results of applying the BBSOC method to the aforementioned maximum crossrange entry vehicle problem are provided in Table 6, where M denotes the number of mesh refinement iterations and K denotes the total number of collocation points. In particular, it is seen from Table 6 that the BBSOC method obtains the same solution as GPOPS – III while taking an average of 0.6 s more CPU time to solve the problem. In particular, the BBSOC method does not identify any discontinuities nor does it identify any intervals as singular. The results obtained for this example demonstrate the ability of the BBSOC method to identify correctly the fact that the optimal control for the maximum crossrange entry vehicle problem is smooth and that the BBSOC method applies only static mesh refinement (see Section 5.2.4) as necessary.

Table 6: Comparison of computational results for Example 5.

	\mathcal{J}^*	M	K	CPU [s]
BBSOC	−0.5963	4	105	1.81
GPOPS – III	−0.5963	4	105	1.17

7 Discussion

The five examples provided in Section 6 illustrate a variety of features of the method developed in this paper. The first example shows that the method accurately solves a problem with a bang-bang optimal control. In particular, for this first example the BBSOC method identifies the locations of discontinuities in the control, partitions the entire domain into the correct number of domains, freezes the control at the

correct limit in each domain, and accurately computes the switch times. The second example demonstrates the ability of the method to identify correctly both bang-bang and singular intervals and to appropriately partition the domain into multiple domains. This second example also demonstrates how the regularization method, used only within a singular domain, iterates to obtain an accurate approximation of the singular control. The third example emphasizes again the ability of the method to identify both bang-bang and singular intervals, this time for a problem whose analytic solution is known. The fourth example shows how the method computes not only an accurate singular control for the case of a finite-order singular arc, but also demonstrates the ability of the method to accurately approximate an infinite-order singular control. Finally, the fifth example shows that the performance of the method is equivalent to the performance of a standard static mesh refinement method in the case where the solution of the optimal control problem is smooth and nonsingular.

8 Conclusions

A method has been described for solving bang-bang and singular optimal control problems using a multiple-domain Radau collocation and regularization of the singular control. First, the solution is approximated on a coarse mesh. Next, structure detection and decomposition is performed via identification of the switch times in the control and use of the switching function to identify any bang-bang and singular arcs. If the structure detected contains discontinuities and bang-bang and/or singular arcs, the structure is partitioned into a multiple-domain formulation with added decision variables to represent the switch times. Then, corresponding constraints and iterative procedures are assigned in each domain type. In bang-bang domains the control is fixed at either its upper or lower limit while in singular domains a regularization method is employed to obtain an accurate approximation of the singular control. Finally, standard mesh refinement is performed if necessary. The strategy of this method allows for highly accurate approximations of the switch times and nonsmooth control without a priori knowledge of the problem structure. The method has been demonstrated on five examples, four of which have either a bang-bang and/or singular optimal control while the fifth has a smooth and nonsingular optimal control. It has been shown that the method developed in this paper provides accurate solutions to problems whose solutions are either bang-bang or singular when

compared against previously developed mesh refinement methods that are not tailored for solving nonsmooth and/or singular optimal control problems, and produces results that are equivalent to those obtained using previously developed mesh refinement methods for optimal control problems whose solutions are smooth.

9 Acknowledgments

The authors gratefully acknowledge support for this research from the U.S. National Science Foundation under grants DMS-1819002 and CMMI-2031213, the U.S. Office of Naval Research under grant N00014-19-1-2543, and from Lockheed-Martin Corporation under contract 4104177872.

References

- [1] Betts, J. T., *Practical methods for optimal control and estimation using nonlinear programming*, SIAM, 2010.
- [2] Biegler, L. T. and Zavala, V. M., “Large-Scale Nonlinear Programming Using IPOPT: An Integrating Framework for Enterprise-Wide Optimization,” *Computers and Chemical Engineering*, Vol. 33, No. 3, March 2008, pp. 575–582.
<https://doi.org/10.1016/j.compchemeng.2008.08.006>.
- [3] Gill, P. E., Murray, W., and Saunders, M. A., “SNOPT: An SQP Algorithm for Large-Scale Constrained Optimization,” *SIAM Review*, Vol. 47, No. 1, January 2002, pp. 99–131.
<https://doi.org/10.1137/S0036144504446096>.
- [4] Benson, D. A., Huntington, G. T., Thorvaldsen, T. P., and Rao, A. V., “Direct Trajectory Optimization and Costate Estimation via an Orthogonal Collocation Method,” *Journal of Guidance, Control, and Dynamics*, Vol. 29, No. 6, November-December 2006, pp. 1435–1440.
<https://doi.org/10.2514/1.20478>.
- [5] Garg, D., Patterson, M. A., Hager, W. W., Rao, A. V., Benson, D. A., and Huntington, G. T., “A Unified Framework for the Numerical Solution of Optimal Control Problems Using Pseudospectral Methods,” *Automatica*, Vol. 46, No. 11, November 2010, pp. 1843–1851.
<https://doi.org/10.1016/j.automatica.2010.06.048>.
- [6] Garg, D., Hager, W. W., and Rao, A. V., “Pseudospectral Methods for Solving Infinite-Horizon Optimal Control Problems,” *Automatica*, Vol. 47, No. 4, April 2011, pp. 829–837.
<https://doi.org/10.1016/j.automatica.2011.01.085>.
- [7] Garg, D., Patterson, M. A., Darby, C. L., Francolin, C., Huntington, G. T., Hager, W. W., and Rao, A. V., “Direct Trajectory Optimization and Costate Estimation of Finite-Horizon and Infinite-Horizon Optimal Control Problems via a Radau Pseudospectral Method,” *Computational Optimization and Applications*, Vol. 49, No. 2, June 2011, pp. 335–358.
<http://dx.doi.org/10.1007/s10589--009--9291--0>.
- [8] Rao, A. V., Benson, D. A., Darby, C. L., Francolin, C., Patterson, M. A., Sanders, I., and Huntington, G. T., “Algorithm 902: GPOPS, A MATLAB Software for Solving Multiple-Phase Optimal Control Problems Using the Gauss Pseudospectral Method,” *ACM Transactions on Mathematical Software*, Vol. 37, No. 2, April–June 2010, Article 22, 39 pages.
<https://doi.org/10.1145/1731022.1731032>.

- [9] Kameswaran, S. and Biegler, L. T., “Convergence Rates for Direct Transcription of Optimal Control Problems Using Collocation at Radau Points,” *Computational Optimization and Applications*, Vol. 41, No. 1, 2008, pp. 81–126.
<https://doi.org/10.1007/s10589--007--9098--9>.
- [10] Patterson, M. A., Hager, W. W., and Rao, A. V., “A hp mesh refinement method for optimal control,” *Optimal Control Applications and Methods*, Vol. 36, No. 4, July–August 2015, pp. 398–421.
<https://doi.org/10.1002/oca.2114>.
- [11] Elnagar, G., Kazemi, M. A., and Razzaghi, M., “The Pseudospectral Legendre Method for Discretizing Optimal Control Problems,” *IEEE transactions on Automatic Control*, Vol. 40, No. 10, 1995, pp. 1793–1796.
<https://doi.org/10.1109/9.467672>.
- [12] Hager, W. W., Hou, H., and Rao, A. V., “Convergence Rate for a Radau Collocation Method Applied to Unconstrained Optimal Control,” 2015.
[arXiv.org/abs/1508.03783](https://arxiv.org/abs/1508.03783).
- [13] Hager, W. W., Hou, H., and Rao, A. V., “Convergence Rate for a Gauss Collocation Method Applied to Unconstrained Optimal Control,” *Journal of Optimization Theory and Applications*, Vol. 169, No. 3, June 2016, pp. 801 – 824.
<https://doi.org/10.1007/s10957--016--0929--7>.
- [14] Hager, W. W., Hou, H., and Rao, A. V., “Lebesgue Constants Arising in a Class of Collocation Methods,” *IMA Journal of Numerical Analysis*, Vol. 37, No. 4, October 2017, pp. 1884–1901.
<https://doi.org/10.1093/imanum/drw060>.
- [15] Hager, W. W., Liu, J., Mohapatra, S., Rao, A. V., and Wang, X.-S., “Convergence rate for a Gauss collocation method applied to constrained optimal control,” *SIAM Journal on Control and Optimization*, Vol. 56, 2018, pp. 1386–1411,
<https://doi.org/10.1137/16M1096761>.
- [16] Hager, W. W., Hou, H., Mohapatra, S., Rao, A. V., and Wang, X.-S., “Convergence rate for a Radau hp-collocation method applied to constrained optimal control,” *Computational Optimization and Applications*, Vol. 74, 2019, pp. 274–314,
<https://doi.org/10.1007/s10589--019--00100--1>.
- [17] Liu, F., Hager, W. W., and Rao, A. V., “Adaptive mesh refinement method for optimal control using nonsmoothness detection and mesh size reduction,” *Journal of the Franklin Institute*, Vol. 352, No. 10, oct 2015, pp. 4081–4106.
<https://doi.org/10.1016/j.jfranklin.2015.05.028>.
- [18] Gong, Q., Fahroo, F., and Ross, I. M., “Spectral Algorithm for Pseudospectral Methods in Optimal Control,” *Journal of Guidance, Control, and Dynamics*, Vol. 31, No. 3, may 2008, pp. 460–471.
<https://doi.org/10.2514/1.32908>.
- [19] Miller, A. T., Hager, W. W., and Rao, A. V., “Mesh refinement method for solving optimal control problems with nonsmooth solutions using jump function approximations,” *Optimal Control Applications and Methods*, 2021.
<https://doi.org/10.1002/oca.2719>.
- [20] Darby, C. L., Hager, W. W., and Rao, A. V., “An hp-adaptive pseudospectral method for solving optimal control problems,” *Optimal Control Applications and Methods*, Vol. 32, No. 4, Aug. 2010, pp. 476–502.
<https://doi.org/10.1002/oca.957>.
- [21] Liu, F., Hager, W. W., and Rao, A. V., “Adaptive Mesh Refinement Method for Optimal Control Using Decay Rates of Legendre Polynomial Coefficients,” *IEEE Transactions on Control Systems Technology*, Vol. 26, No. 4, July 2018, pp. 1475–1483,
<https://doi.org/10.1109/tcst.2017.2702122>.

- [22] Schlegel, M. and Marquardt, W., “Direct Sequential Dynamic Optimization with Automatic Switching Structure Detection,” *IFAC Proceedings Volumes*, Vol. 37, No. 9, July 2004, pp. 419–424.
[https://doi.org/10.1016/s1474-6670\(17\)31845-1](https://doi.org/10.1016/s1474-6670(17)31845-1).
- [23] Schlegel, M. and Marquardt, W., “Detection and exploitation of the control switching structure in the solution of dynamic optimization problems,” *Journal of Process Control*, Vol. 16, No. 3, March 2006, pp. 275–290.
<https://doi.org/10.1016/j.jprocont.2005.06.008>.
- [24] Wang, P., Yang, C., and Yuan, Z., “The Combination of Adaptive Pseudospectral Method and Structure Detection Procedure for Solving Dynamic Optimization Problems with Discontinuous Control Profiles,” *Industrial & Engineering Chemistry Research*, Vol. 53, No. 17, April 2014, pp. 7066–7078.
<https://doi.org/10.1021/ie404148j>.
- [25] Chen, W. and Biegler, L. T., “Nested direct transcription optimization for singular optimal control problems,” *AIChE Journal*, Vol. 62, No. 10, May 2016, pp. 3611–3627.
<https://doi.org/10.1002/aic.15272>.
- [26] Chen, W., Ren, Y., Zhang, G., and Biegler, L. T., “A simultaneous approach for singular optimal control based on partial moving grid,” *AIChE Journal*, Vol. 65, No. 6, March 2019, pp. e16584.
<https://doi.org/10.1002/aic.16584>.
- [27] Agamawi, Y. M., Hager, W. W., and Rao, A. V., “Mesh refinement method for solving bang-bang optimal control problems using direct collocation,” *AIAA Scitech 2020 Forum*, 2020, pp. 0378.
<https://doi.org/10.2514/6.2017-1506>.
- [28] Aghaee, M. and Hager, W. W., “The Switch Point Algorithm,” 2021.
<https://arxiv.org/abs/2011.10022>.
- [29] Kaya, C. and Noakes, J., “Computational Method for Time-Optimal Switching Control,” *Journal of Optimization Theory and Applications*, Vol. 117, No. 1, April 2003, pp. 69–92.
<https://doi.org/10.1023/a:1023600422807>.
- [30] Mehrpouya, M. A. and Khaksar-e Oshagh, M., “An efficient numerical solution for time switching optimal control problems,” *Computational Methods for Differential Equations*, Vol. 9, No. 1, Jan. 2021.
<https://doi.org/10.22034/cmde.2020.33529.1542>.
- [31] Maurer, H., “Numerical solution of singular control problems using multiple shooting techniques,” *Journal of Optimization Theory and Applications*, Vol. 18, No. 2, feb 1976, pp. 235–257.
<https://doi.org/10.1007/bf00935706>.
- [32] Aronna, M. S., Bonnans, J. F., and Martinon, P., “A Shooting Algorithm for Optimal Control Problems with Singular Arcs,” *Journal of Optimization Theory and Applications*, Vol. 158, No. 2, Jan. 2013, pp. 419–459.
<https://doi.org/10.1007/s10957-012-0254-8>.
- [33] Mehra, R. and Davis, R., “A generalized gradient method for optimal control problems with inequality constraints and singular arcs,” *IEEE Transactions on Automatic Control*, Vol. 17, No. 1, Feb. 1972, pp. 69–79.
<https://doi.org/10.1109/tac.1972.1099881>.
- [34] Jacobson, D., Gershwin, S., and Lele, M., “Computation of optimal singular controls,” *IEEE Transactions on Automatic Control*, Vol. 15, No. 1, feb 1970, pp. 67–73.
<https://doi.org/10.1109/tac.1970.1099360>.
- [35] Andrés-Martínez, O., Flores-Tlacuahuac, A., Kameswaran, S., and Biegler, L. T., “An efficient direct/indirect transcription approach for singular optimal control,” *AIChE Journal*, Vol. 65, No. 3, Dec. 2018, pp. 937–946.
<https://doi.org/10.1002/aic.16487>.

- [36] Caponigro, M., Ghezzi, R., Piccoli, B., and Trélat, E., “Regularization of chattering phenomena via bounded variation controls,” *IEEE Transactions on Automatic Control*, Vol. 63, No. 7, 2018, pp. 2046–2060.
<https://doi.org/10.1109/TAC.2018.2810540>.
- [37] Mall, K., Grant, M. J., and Taheri, E., “Uniform Trigonometric Method for Optimal Control Problems with Control and State Constraints,” *Journal of Spacecraft and Rockets*, Vol. 57, No. 5, Sept. 2020, pp. 995–1007.
<https://doi.org/10.2514/1.a34624>.
- [38] Fabien, B. C., “Indirect Solution of Inequality Constrained and Singular Optimal Control Problems Via a Simple Continuation Method,” *Journal of Dynamic Systems, Measurement, and Control*, Vol. 136, No. 2, nov 2013, pp. 021003.
<https://doi.org/10.1115/1.4025596>.
- [39] Andrés-Martínez, O., Biegler, L. T., and Flores-Tlacuahuac, A., “An indirect approach for singular optimal control problems,” *Computers & Chemical Engineering*, Vol. 139, Aug. 2020, pp. 106923.
<https://doi.org/10.1016/j.compchemeng.2020.106923>.
- [40] Maga, L., Reverberi, A., et al., “A pattern recognition approach to the solution of optimal singular control problems,” *Chemical Engineering Journal*, Vol. 68, No. 1, 1997, pp. 35–40.
[https://doi.org/10.1016/S1385-8947\(97\)00068-5](https://doi.org/10.1016/S1385-8947(97)00068-5).
- [41] Pager, E. R. and Rao, A. V., “A Proximal Method for the Numerical Solution of Singular Optimal Control Problems Using a Modified Radau Collocation Method,” *AIAA Scitech 2020 Forum*, American Institute of Aeronautics and Astronautics, Jan. 2020.
<https://doi.org/10.2514/6.2020-0377>.
- [42] Pager, E. R. and Rao, A. V., “A Method for the Numerical Solution of Singular Optimal Control Problems Using an Adaptive Radau Collocation Method,” *AIAA Scitech 2021 Forum*, American Institute of Aeronautics and Astronautics, Jan. 2021.
<https://doi.org/10.2514/6.2021-1456>.
- [43] Athans, M. and Falb, P. L., *Optimal control: an introduction to the theory and its applications*, Courier Corporation, 2013.
- [44] Kirk, D. E., *Optimal control theory: an introduction*, Courier Corporation, 2004.
- [45] Bryson, A. E. and Ho, Y., *Applied Optimal Control: Optimization, Estimation, and Control*, Hemisphere Publishing Corporation, 1975.
- [46] Pontryagin, L. S., *Mathematical theory of optimal processes*, Routledge, 2018.
- [47] Bazaraa, M. S., Sherali, H. D., and Shetty, C. M., *Nonlinear programming: theory and algorithms*, John Wiley & Sons, 2013.
- [48] Bertsekas, D. P. et al., *Dynamic programming and optimal control: Vol. 1*, Athena scientific Belmont, 2000.
- [49] Kelley, H., Kopp, R. E., and Moyer, H. G., “Topics in Optimization, edited by Leitman,” 1967.
- [50] Kopp, R. E. and Moyer, H. G., “Necessary conditions for singular extremals,” *AIAA Journal*, Vol. 3, No. 8, Aug. 1965, pp. 1439–1444.
<https://doi.org/10.2514/3.3165>.
- [51] Archibald, R., Gelb, A., and Yoon, J., “Polynomial Fitting for Edge Detection in Irregularly Sampled Signals and Images,” *SIAM Journal on Numerical Analysis*, Vol. 43, No. 1, Jan. 2005, pp. 259–279.
<https://doi.org/10.1137/s0036142903435259>.
- [52] Fritsch, F. N. and Carlson, R. E., “Monotone Piecewise Cubic Interpolation,” *SIAM Journal on Numerical Analysis*, Vol. 17, No. 2, April 1980, pp. 238–246.
<https://doi.org/10.1137/0717021>.

- [53] Patterson, M. A. and Rao, A. V., “GPOPS-II,” *ACM Transactions on Mathematical Software*, Vol. 41, No. 1, oct 2014, pp. 1–37.
<https://doi.org/10.1145/2558904>.
- [54] Weinstein, M. J. and Rao, A. V., “Algorithm 984: ADiGator, a Toolbox for the Algorithmic Differentiation of Mathematical Functions in MATLAB Using Source Transformation via Operator Overloading,” *ACM Transactions on Mathematical Software*, Vol. 44, No. 2, Aug. 2017, pp. 1–25.
<https://doi.org/10.1145/3104990>.
- [55] Dolan, E. D., More, J. J., and Munson, T. S., “Benchmarking optimization software with COPS 3.0.” Tech. rep., Argonne National Laboratory, Argonne, Illinois, May 2004.
<https://doi.org/10.2172/834714>.
- [56] Aly, G., “The computation of optimal singular control,” *International Journal of Control*, Vol. 28, No. 5, 1978, pp. 681–688.
<https://doi.org/10.1080/00207177808922489>.
- [57] Shen, H. and Tsiotras, P., “Time-Optimal Control of Axisymmetric Rigid Spacecraft Using Two Controls,” *Journal of Guidance, Control, and Dynamics*, Vol. 22, No. 5, Sept. 1999, pp. 682–694.
<https://doi.org/10.2514/2.4436>.